♦ IS-95 Enhancements for Multimedia Services

Chih-Lin I, Charles A. Webb III, Howard C. Huang, Stephan ten Brink, Sanjiv Nanda, and Richard D. Gitlin

Existing code division multiple access (CDMA) systems, such as the IS-95 digital cellular system, support data and voice traffic at a basic rate as well as lower fractional rates. A backward-compatible system, known as multicode CDMA (MC-CDMA), has been proposed as a mechanism to allow higher-rate services under the IS-95 infrastructure. MC-CDMA enables dynamic packet-like user access with low overhead and high efficiency. This paper describes MC-CDMA and focuses on several issues related to its implementation, exploring both high-level system design and details of hardware implementation. The load- and interference-based demand assignment (LIDA) access control mechanism allows dynamic data rate access by balancing and controlling mixed traffic interference in a CDMA system. LIDA builds on existing pilot measurement and soft handoff protocols and thus can be integrated easily with IS-95. Also discussed are forward link interference suppression schemes that mitigate multipath impairments, resulting in increased capacity and/or improving quality. The paper concludes by describing an efficient design for a bidirectional 56-kb/s MC-CDMA mobile transceiver that requires only minimally increased complexity when compared with a conventional CDMA tranceiver. Together with all these enhancements, MC-CDMA provides a simple and effective transition mechanism for future wireless multimedia services.

Introduction

Code division multiple access (CDMA) technology has gained significant attention in recent years as a prominent technology for wireless networks,[1,2,3] and it forms the basis for the IS-95 digital cellular systems now being introduced worldwide. Compared to other technologies, CDMA has many characteristics that make it very attractive for voice telephony. In contrast to orthogonal systems, such as time division multiple access (TDMA) and frequency division multiple access (FDMA) technologies, CDMA requires neither frequency planning among cells nor orthogonality coordination among users within a cell. In addition, CDMA systems have inherent frequency diversity to counteract multipath impairments, as well as the ability to exploit the advantages of voice activity factor and antenna sectorization. Because of these advantages, the cellular industry—both vendors and service providers—has invested heavily in CDMA technology. This paper discusses enhancements to existing CDMA systems that enable bandwidth-on-demand multimedia applications. The goal is to work within the framework of existing CDMA systems without making significant changes that would require costly hardware or software modifications.

The initial motivation is to provide a cellular digital packet data (CDPD)-like capability—that is, a packet data overlay on the analog cellular network. Many services have been identified, and while some of them require rates in excess of 100 kb/s, it is recognized that wireless data rates in the range of 56 to 64 kb/s are of great importance and interest. These rates are well above the 19.2-kb/s rate (10 to 12 kb/s actual

throughput) CDPD provides, and they match the data rates on the public switched packet data network (for example, X.25). Moreover, with the emerging availability of a mobile video telephony coder at 28.8 kb/s, such as H.324m,[4] a true multimedia connection can be enabled at 56 kb/s. Finally, at these rates, Internet surfing over a wide-area wireless network becomes viable.

At the request of cellular and personal communications services (PCS) providers, the CDMA development group (CDG), with representatives from various sectors of the CDMA industry, is working on a higher speed data-service option under the existing IS-95 infrastructure. The CDG has established 64-kb/s high-speed data as the first targeted enhancement.

The multicode CDMA (MC-CDMA) system[5] is a packet-based wireless network that accommodates multimedia traffic. It was conceived to provide a smooth migratory path to PCS either from a digital cellular system (IS-95) or from a wideband CDMA system to serve both isochronous and asynchronous applications. MC-CDMA maintains a large spreading gain even for users having a very high application data rate. The additional processing required as compared with a conventional CDMA system is primarily in the baseband. The subcode concatenation scheme not only eliminates a user's self-interference but also simplifies code negotiation by building on the standardized user long-code assignment procedures in IS-95.

Few constraints are imposed on MC-CDMA technology in terms of the baseline CDMA system. However, considering what exists today and the PCS-spectrum license regulation, the two natural candidate baseline systems are the IS-95 1.25-MHz CDMA system and a wideband 5-MHz CDMA system.[6] This paper focuses on IS-95 evolution through MC-CDMA, exploring both high-level system design issues and lower-level hardware implications.

One of the major challenges in cellular CDMA systems supporting mixed traffic is the potentially high outage probability.[7] This problem is a result of large intercell interference variations caused by high data-rate users. To remedy such problems, a demand assignment access scheme was proposed, called the load- and interference-based demand assignment (LIDA).[8] This paper discusses the LIDA access control mechanism and shows how multimedia traffic can be supported in an enhanced IS-95 system by extending the pilot measurement and soft hand-off functionality.

From a hardware standpoint, the mobile terminal's design is the most challenging. Unlike the base station, the mobile terminal does not already have multichannel processing capability. The paper presents some enhancements and optimizations that minimize the impact of MC-CDMA on the mobile terminal's design. It highlights, for example, an efficient MC-CDMA receiver design that minimizes increased complexity.

The sections that follow introduce the MC-CDMA system, briefly explain the physical-layer implementation aspects of the base station, and dis-

Panel 1. Abbreviations, Acronyms, and Terms

AGC—automatic gain control
ASIC—application-specific integrated circuit
BER—bit error rate
BPSK—binary phase shift keying
CDG—CDMA development group
CDMA—code division multiple access
CDPD—cellular digital packet data
DSP—digital signal processor
FDMA—frequency division multiple access
FIR—finite impulse response
i.i.d.—independent and identically distributed
IS—interference subtraction
LIDA—load- and interference-based demand assignment
MC-CDMA—multicode CDMA
O-QPSK—offset quadrature phase shift keying
PCS—personal communications services
PD—partial decorrelation
QOS—quality of service
QPSK—quadrature phase shift keying
RF—radio frequency
RLPF—reconstruction low-pass filter
RSSI—received signal-strength indicator
SNR—signal-to-noise ratio
SRAM—static random access memory
TDMA—time division multiple access
WH—Walsh-Hadamard

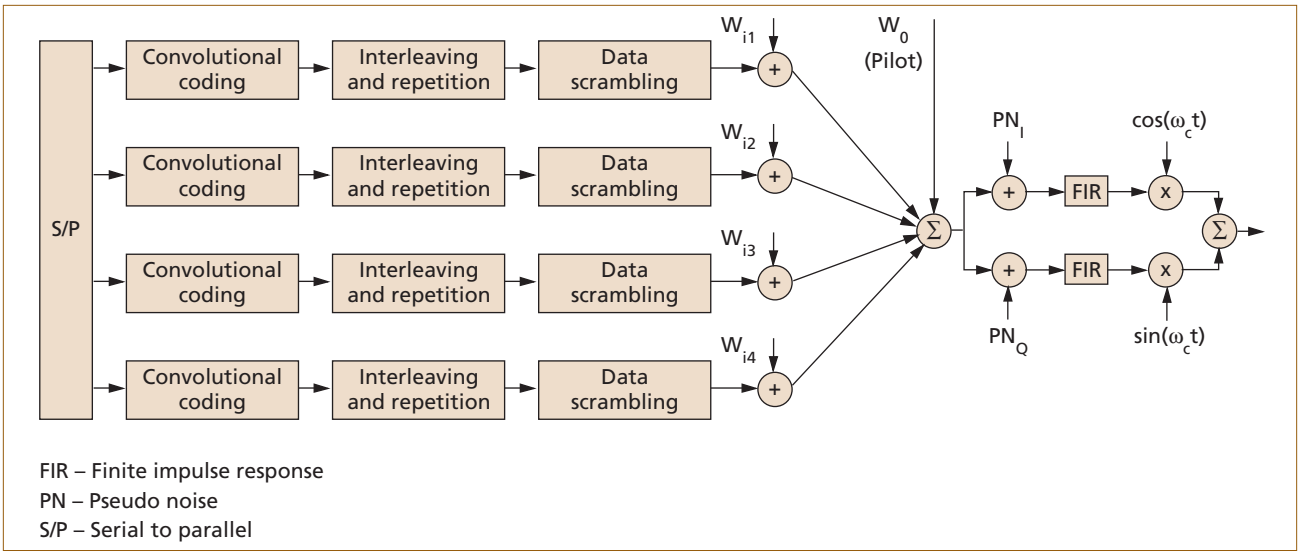

Figure 1.
Simplified block diagram of an MC-CDMA forward link transmitter (N = 4).

cuss LIDA. Mobile terminal enhancements are presented, including the MC-CDMA rake receiver and forward-link interference cancellation. The paper concludes with a synopsis of the impact MC-CDMA has on existing mobile terminals, some specific design examples, and a summary of our research to date.

MC-CDMA

Because many services (for example, voice, data, image, and perhaps video) are expected to be implemented in future wireless networks, users having different time-varying source rates must be accommodated. A CDMA-based system called MC-CDMA was recently proposed.[5,6] The system provides a smooth migratory path from existing CDMA systems by maintaining much of the existing physical-layer protocols, and it can also be adapted to other proposed wideband CDMA systems. MC-CDMA is a wireless system whose rates and services are dynamically matched to users' needs. It can evolve from existing IS-95 CDMA systems, and it differs in that multiple code channels and, hence, increased data rates can be assigned to a single user. By allocating these codes to users as needed, a unified digital bandwidth-on-demand platform can be realized.

When an MC-CDMA user needs (and is allowed by the controller) N times the basic source rate, it converts its signal stream—serial to parallel—into N basic rate streams, encodes each stream with a different code, and superimposes them before upconverting for radio transmission. The scheme retains the CDMA advantage in counteracting multipath distortion and is compatible with existing base station hardware.

The next two subsections present the transmitter architectures of both coherent MC-CDMA (typically for the forward link) and noncoherent MC-CDMA (typically for the reverse link), as well as their key features.

MC-CDMA Forward Link

In current IS-95 CDMA systems, a base station transmits data to each mobile user over one of 64 orthogonal Walsh channels. Applying MC-CDMA to this link can be accomplished by simply grouping multiple Walsh channels for mobile users that require higher data-rate services. No hardware changes are required at the base station transmitter. **Figure 1**, a simplified block diagram, depicts a user who has been allocated four basic-rate forward Walsh channels.

Sequences PN_I and PN_Q are codes used to identify the base station. All users in a cell have the same pair of base station codes. N is a variable that denotes the data rate transmitted to a user as a multiple of the basic rate ($N = 1$ means that the base station is transmitting at the basic rate). N also represents the number of parallel Walsh channels that are grouped together to serve a high-rate mobile user. Multiple Walsh chan-

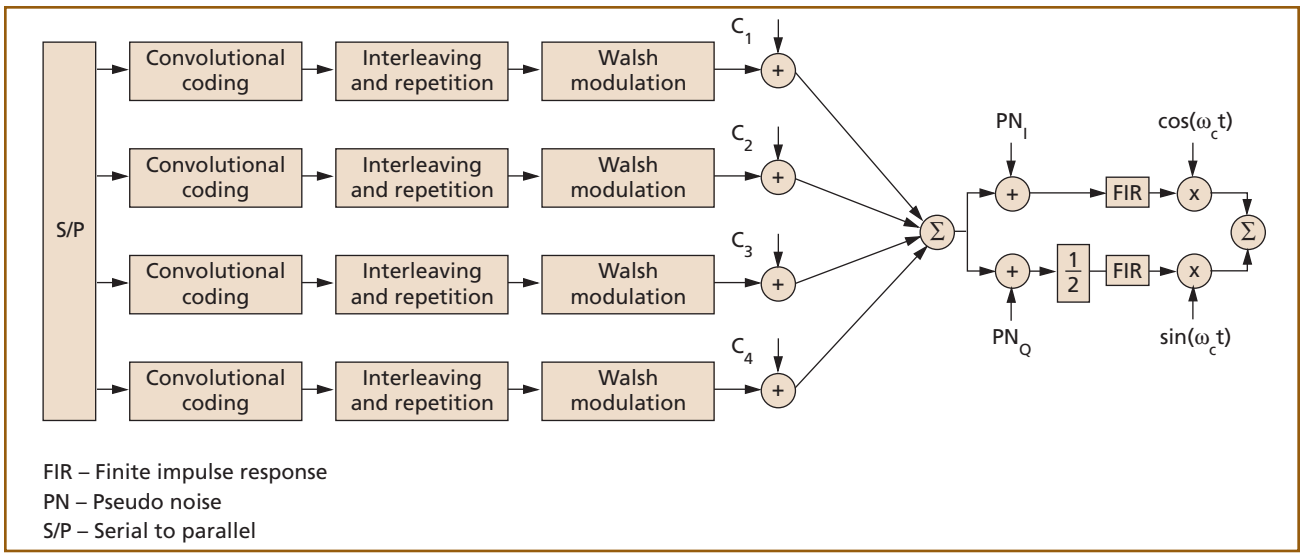

Figure 2.
Simplified block diagram of an MC-CDMA reverse-link transmitter (N = 4).

nels grouped for a user can be any subset of the 64 channels. Judicious selection of Walsh channels can reduce mobile receiver complexity.[9] However, this may also increase system-level complexity related to additional intra-sector handoffs. In the "Fat Fingers" subsection, we present mobile receiver designs both with and without the advantages of such judicious selection of Walsh channels.

A more futuristic version of the MC-CDMA forward link may use quadrature phase shift keying (QPSK) modulation instead of the current binary phase shift keying (BPSK). Again building on IS-95, a configuration similar to that shown in Figure 1 can support a user at $2N = 8$ times the basic rate.

MC-CDMA Reverse Link

In contrast to the forward link, which uses orthogonal codes and coherent detection, the IS-95 reverse link employs nonorthogonal codes and noncoherent detection. Users (channels) are distinguished by adopting different pseudo-random codes. Building on a conventional CDMA system, **Figure 2** illustrates the MC-CDMA reverse-link architecture. N denotes the data rate transmitted by a user as a multiple of the basic rate, and it is also the number of active parallel branches.

In Figure 2, sequences C_i's are the random spreading codes a user employs in parallel when transmitting at a rate higher than the basic rate. These codes can be generated either by code aggregation or subcode concatenation as defined below:

- *Code aggregation*. A simple method of implementing MC-CDMA is to allocate multiple long PN code masks to a single user. We refer to this approach as code aggregation because it simply aggregates multiple non-orthogonal basic rate channels to that user. Code aggregation has an advantage in that it requires no modification to existing receiver hardware at the base station. However, a performance penalty due to self-interference results because the aggregated codes are not orthogonal to one another.
- *Subcode concatenation*. To avoid the self-interference that an MC-CDMA user may incur, we propose a subcode concatenation scheme.[5] Each user admitted into the system has a unique primary code, such as the long PN code, assigned to it. The primary codes of different users are PN codes—that is, they are not orthogonal among different users. The multiple codes from one user can and should be made orthogonal. If C_1 is the primary code of a user and the user requires a higher rate, the additional codes, C_i, are derived from C_1 by $C_i = C_1 \oplus D_i$, where $D_i \perp D_j$, $i \neq j$. Obviously, $C_i \perp C_j$, $i \neq j$.

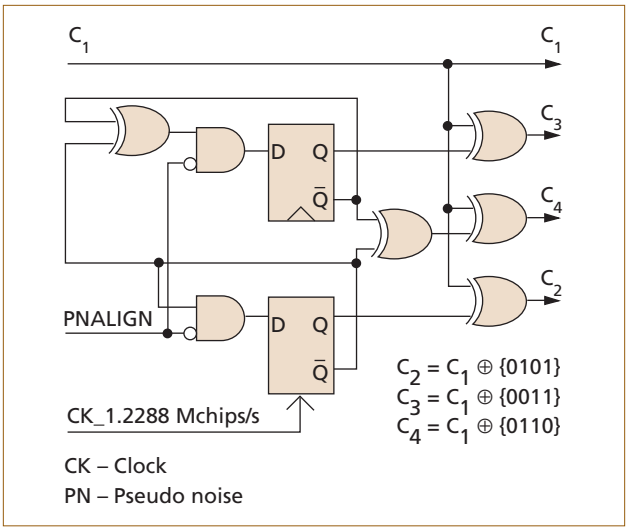

Figure 3.
Subcode generator.

Figure 3 depicts a simple subcode generator with $N = 4$, which can be implemented in fewer than 100 logic gates. Its complexity is extremely low. The orthogonality is maintained at the receiver because the propagation variations on the parallel codes are the same. In addition to eliminating self-interference on the same path, this scheme simplifies dynamic access since explicit multiple code negotiation is not needed.

Both code aggregation and subcode concatenation transmit a signal that is the superposition of several basic rate offset QPSK (O-QPSK) signals. Such a signal has a greater peak/average ratio and thus requires a more linear power amplifier. For the case of $N = 4$ basic rate O-QPSK channels, the power amplifier must have a linear range that is 2.7 dB greater than current amplifiers.

Given all the variables for implementing an MC-CDMA system, several viable candidate systems have been investigated.[6] **Table I** shows six candidate MC-CDMA systems. We assume that the reverse link employs subcode concatenation for all six systems. The maximum data rate for each system is determined by the orthogonality requirements among the multiple codes. We concentrate on candidate system Q3, which offers a maximum data rate of 57.6 kb/s for the reverse link by using $N = 4$ subcodes.

Figure 4 shows a corresponding reverse-link receiver architecture at the base station. This architecture requires simply the addition of a subcode generator to the existing hardware. The search finger of only one basic receiver must be active or one may jointly run the N searcher fingers for improved efficiency.

MC-CDMA Features

To facilitate the receiver design, we observe the following key features[5] of the MC-CDMA architecture. Although also true for the reverse link, they are particularly important for the forward link.

- *Rate quantization*. On the transmitter side, the

Table I. Candidate MC-CDMA configurations.

Candidate System	Q1	A1	Q2	A2	Q3	A3
Bandwidth (MHz)	1.25	5	1.25	5	1.25	5
Vocoder (kb/s)	8	8	8	8	13	13
Voice ECC rate	1/3	1/3	1/3	1/3	1/2	1/2
Voice path Walsh	64	64	64	64	64	64
Voice QOS (dB)	7	7	7	7	7.5	7.5
Basic data rate (kb/s)	9.6	9.6	19.2	19.2	14.4	14.4
Data ECC rate	1/3	1/3	1/2	1/2	1/2	1/2
Data path Walsh	64	64	16	16	64	64
Data QOS (dB)	9	9	10.5	10.5	9.5	9.5
Max. data rate (kb/s)	38.4	153.6	153.6	614.4	57.6	230.4

ECC – Error correction code
QOS – Quality of service

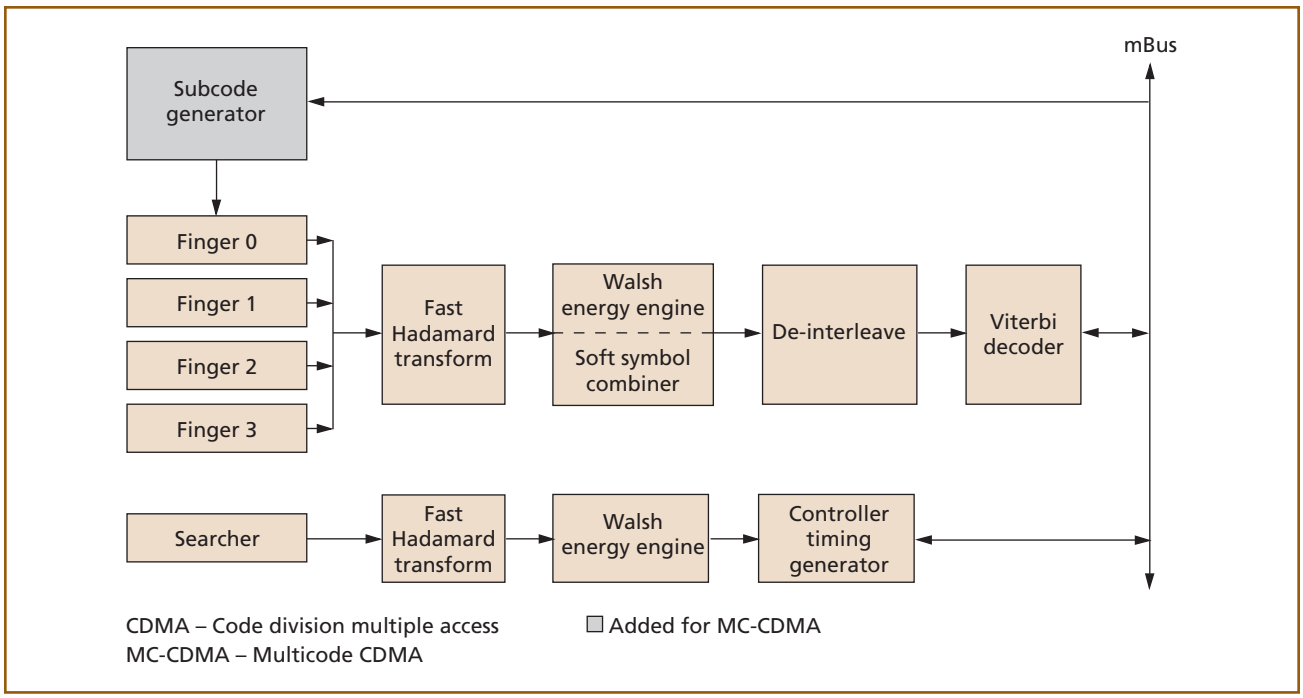

Figure 4.
Reverse-link receiver architecture.

actual user rate does not have to be an integer multiple of the basic rate. Each code in MC-CDMA carries a basic rate. N codes in parallel will provide a single user N times the basic rate capability. If one of the codes (that is, the primary code) is equipped with subrate capability (for example, variable spreading gain to provide 1/2 rate or 1/4 rate as for voice in IS-95), then much finer quantization is possible in terms of the rate offering to a user. Because the fractional rate is always carried by the first (primary) code, the additional codes carry data only at the full rate. By doing so, the rate detection algorithm for multiple rate detection is needed only on the primary channel.

- *Synchronization/acquisition*. On the receiver side, the synchronization/acquisition subsystem is very demanding even for regular CDMA systems. The good news is that the MC-CDMA receiver does not require an N-fold complexity increase in synchronization/acquisition. Because the parallel codes all suffer the same impairments, one searcher circuit will suffice for all the parallel codes. We will elaborate on this point in the section "Performance and Complexity Optimizations for the MC-CDMA Mobile Receiver."

Dynamic Access Control

The dynamic packet-like capacity access enabled by MC-CDMA allows users to access the base station at different data rates. Additionally, MC-CDMA will provide peak rate access to a single user when other users are idle. With appropriate access control, it will enable efficient delivery of all services made possible by digital cellular, CDPD, and other PCS technologies.

Two fundamentally different approaches can be used, however, for dynamic access between bursts in an MC-CDMA system—namely, *probabilistic access* and *demand assigned access*. Taking a probabilistic approach, adaptive access control, which has been proposed,[10] can be employed. The base station broadcasts the current uplink load information. Users having bursts to transmit will then make probabilistic decisions on whether to transmit, either to optimize the conditional expected load or the conditional probability of the system overload given the current load. Priority for

users with ongoing bursts over users with new bursts can be incorporated in this control mechanism.[10] Furthermore, instead of a decision on whether or not to transmit given the current load information, a user can decide to transmit at a lower yet nonzero rate.

The probabilistic approach is attractive in that user access can be instantaneous, and no central controller is required to assign spectral resources dynamically among users in a cell. Users can reserve common codes for burst access (as in IS-95 access channels). This scheme can be inefficient, however, because the time needed to reacquire synchronization and power control for every burst may be long. For example, the initial access burst in IS-95 has an acquisition preamble that is 20- to 80-ms long.

Taking a demand assignment approach, users with bursts to transmit or those with increased data rates must make requests and wait for assignment. In orthogonal systems, the assignment (for example, with RAMA/TRAMA access protocols[11-13]) is to specify time slots and/or carriers to the user. As discussed in the "MC-CDMA" section, each user has a unique primary code assigned at call setup time. Thus, only the number of codes must be dynamically assigned.[5] When a user is idle, a very low fractional-rate signaling channel is maintained using its primary code to facilitate synchronization and power control procedures. The primary channel is also used to make burst access requests prior to a burst transmission.

On receiving the rate assignment from the base station, the user adopts subcode concatenation to generate locally the corresponding number of codes for its transmission while the receiver at the base station does the same. The user, then, transmits at a power level adjusted according to the number of codes used, as well as the QOS required. The low-rate maintenance channel assures continuous synchronization and power control and provides a dedicated signaling (access request) channel with low overhead.

LIDA

This subsection discusses the LIDA network control scheme,[7,8] which protects voice users in a public network with burst-level demand assigned access for high-bandwidth users.

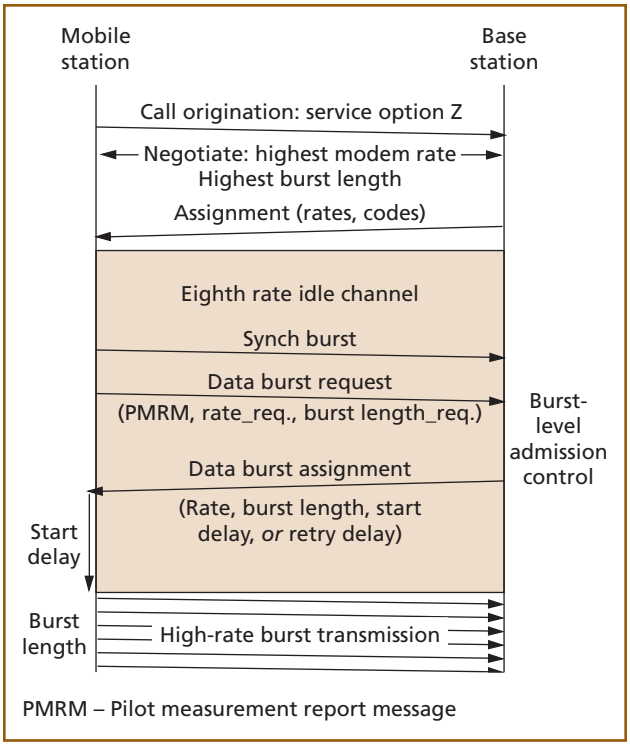

Figure 5.
Flow diagram for LIDA.

We begin by examining mobile terminal-assisted soft hand-off in current CDMA systems. The base station provides the mobile terminal with a neighbor list of pilots. The mobile periodically measures the pilot strength on its neighbor list and transmits it to the base station. If the pilot strength of a base station to which the mobile is not connected is greater than a threshold T_{add}, the base station initiates a soft hand-off to the strong base station for the mobile station. The "Burst request" subsection extends the use of pilot strength measurements to access control of high-data-rate users.

Burst request. The control flow of LIDA is shown in **Figure 5**. A unique primary code is assigned to each admitted user at call setup. When a user is quiescent, a very-low-rate (say, eighth rate) signaling channel is maintained using the primary code. This subrate channel helps maintain synchronization and coarse power control. It is maintained whether the user is "connected'' to one base station or is in soft handoff with multiple cells. Because the transmission during eighth-rate frames is intermittent, both the synchronization and power control may be

inadequate if the quiescent period is long. Hence, any transmission from the mobile terminal after a long quiescent period may be lost. This can be fixed easily by requiring the mobile terminal to transmit one (or more) idle basic-rate frames at the end of a long quiescent period. Following the idle frame(s) that give the receiver time to synchronize and provide power-control feedback, the mobile terminal signals a request for data transmission using signaling messages over the basic-rate channel. Alternately, instead of the idle frames, the mobile terminal could be required to transmit the request multiple times.

The access request from the mobile terminal contains both the data rate and burst length requested. The maximum burst length that may be requested is specified by the system (and is chosen to best coordinate shared access between users). In addition, to provide interference information to the base station, the mobile terminal must include pilot strength information (for cells in its neighbor list) within the access request. The inclusion of the pilot strength measurements within the access request is independent of (and in addition to) any such reports used for handling soft handoffs. The pilot strength measurements received from the mobile terminal indicate to the base station the interference levels that will be seen at both the base station and its neighbors due to transmissions from the mobile terminal. This measure of interference accounts for both distance loss and shadow fading. Thus, the interference level is a measure of radio distance, which is used to make access control decisions in LIDA.

Bandwidth tradeoffs. Simulation and analysis of bandwidth tradeoffs have been undertaken. Providing four multiple codes to a single user without appropriate control may incur a capacity penalty in the range of 10 to 15% from a straightforward outage computation. LIDA maintains sufficient voice capacity per sector by controlling the burst access of higher data-rate users, and its algorithms provide sufficient network control to achieve favorable tradeoffs among voice and data users. Further results will be presented in a subsequent paper.

Classification of LIDA Algorithms

Once the burst request is received at the base station, the network must coordinate access with other requests, as well as with the voice load already offered to the system. We have defined several access-control mechanisms having varying amounts of complexity using the LIDA procedure. The simplest process is implemented autonomously by each base station. More general procedures require access coordination between neighbor base stations, including instantaneous loading information about neighbor cells. Light loading in neighbor cells can be exploited to permit higher-rate access while still meeting interference constraints. To allow burst access at rates up to N times the basic rate, LIDA algorithms are generally based on three factors:

- Load information in the cell and its neighbors;
- Pilot strength measurements provided by the mobile terminal; and
- Coordination of the burst rate, burst length, and burst starting time between neighbor cells.

A brief description of some LIDA algorithms having various levels of complexity follows. Additional details, however, are available.[8] Throughput and delay performance, as well as implementation and complexity issues, are the subjects of ongoing research.

- *One threshold, basic rate in soft handoff.* If the pilot strength measurements for all neighbors are below a high-rate data access threshold T_N that indicates the mobile terminal will not cause any excess interference to neighboring base stations, then the mobile terminal is permitted to transmit at N times the basic rate. If any one of the neighbor pilots is higher than the threshold, the mobile terminal is permitted to transmit only at the basic rate. To accommodate high-rate data users, the number of voice users per cell may be reduced.
- *M thresholds, basic rate in soft handoff.* By creating multiple thresholds, we can increase the coverage area for higher-rate data users such that rates 2, 3, ... times higher than the basic rate can be assigned. N pilot strength thresholds are defined corresponding to different multiples of the basic rate.
- *Neighbor-coordinated access control.* If the base station "knows" the load at the neighbor cells,

instead of fixed thresholds, the base station can make rate assignment decisions by determining the largest multiple of the basic rate that satisfies the interference constraints at all neighbor base stations. In this case, additional communication is required for the neighbor cells to provide periodic updates of their current load.

- *Soft hand-off coordination*. When the mobile terminal is in the soft hand-off state, each connected base station performs similar threshold comparisons or computations as discussed above to determine the maximum permitted rate. Base stations then forward this value to the central controller for the call. The controller compares the assignment made by each base station, chooses the minimum rate assignment, and transmits it to the mobile terminal in soft handoff.

Performance and Complexity Optimizations for the MC-CDMA Mobile Receiver

The implementation and hardware design of an MC-CDMA system is more challenging at the mobile terminal than at the base station because of the limited computational resources at the former. In this section, we first discuss methods that minimize the computational complexity of an MC-CDMA receiver at the mobile terminal. Next, we show how interference cancellation techniques can improve detector performance and thereby increase capacity. Specifically, we show how low-complexity cancellation techniques increase the downlink capacity of a conventional (non-MC) IS-95 system by 12.5% and an MC-CDMA system by 17.5% at 3×10^{-3} BER.

Fat Fingers

As previously suggested, the receiver of a multicode user does not need N times the complexity to support N times the basic data rate. In particular, the same synchronization and timing circuitry is shared among multiple codes. Thus, neither the rake receiver nor the fingers that constitute the rake need to be replicated for each code. To minimize receiver complexity in terms of hardware cost, power consumption, and design effort, we propose three designs that exploit characteristics available in all MC-CDMA systems. In all three designs discussed in this subsection, the computational savings translate into hardware and/or power savings that are important for a mobile terminal.

The first design, known as the *fat finger*, tracks and acquires multiple Walsh code channels with a single timing and synchronization unit. It employs fingers with multiple complex correlators, adding one complex correlator per finger for each additional Walsh code channel being received. This design saves $2(N-1)$ complex correlators in a coherent receiver compared to a more straightforward implementation, which might use a larger number of conventional fingers. A similar approach can be applied to noncoherent receivers with slightly different results. A specific example of this design is presented in the section "MC-CDMA Handset ASIC at 56 kb/s."

The second design, called the *skinny fat finger*, allows for further complexity reduction assuming the N codes are chosen to satisfy the following relationship. Because generalizing to other N (where N is an integer power of 2) is straightforward, we simply consider the $N = 4$ MC channel case. Let w(n) be the n^{th} ($n = 1...4$) Walsh code of length N_c (the number of chips per bit interval). The Walsh codes for the four MC channels are assigned by the base station such that the four-chip sub-sequences in each of the codes satisfy the following order-4 Walsh-Hadamard (WH) relationship:

$$\begin{aligned} \mathbf{w}(1) &= [\mathbf{x}\,\mathbf{x}\,\mathbf{x}\,\mathbf{x}] \\ \mathbf{w}(2) &= [\mathbf{x}\,\bar{\mathbf{x}}\,\mathbf{x}\,\bar{\mathbf{x}}] \\ \mathbf{w}(3) &= [\mathbf{x}\,\mathbf{x}\,\bar{\mathbf{x}}\,\bar{\mathbf{x}}] \\ \mathbf{w}(4) &= [\mathbf{x}\,\bar{\mathbf{x}}\,\bar{\mathbf{x}}\,\mathbf{x}], \end{aligned} \tag{1}$$

where $\mathbf{x}$ represents an arbitrary $N_c/4$ length subsequence and $\bar{\mathbf{x}}$ represents its modulo-2 inverse. For a given bit interval, a single matched filter correlates the four $N_c/4$-chip groups of the received signal with the subsequence $\mathbf{x}$. To obtain the overall correlation output for each MC channel, the N intermediate correlation results are appropriately combined using additions and subtractions according to their respective Walsh code subsequences. Because the Walsh sequences were chosen to satisfy the specific WH relationship in (1), the combining for the N final correlator results can

be computed efficiently using a fast WH transformation of order N[16] on the N intermediate correlation results. Compared to the fat finger receiver, which requires $N \cdot N_C$ complex additions per symbol period, the low fat finger requires only $N_C + N \cdot \log_2 N$ complex operations per symbol.

A third mechanism for reducing the hardware complexity of an MC-CDMA rake receiver finger is to share common logic among the complex correlators within a finger and time-multiplexing the use of a single adder to implement the accumulators for multiple complex correlators. This is done by exploiting the fact that existing timing generators for a finger divide a single chip into several higher frequency ticks to account for multipath delays, which are fractions of a chip interval. One accumulation for a complex correlator can occur during each of these ticks. This sharing mechanism, which replaces N chip-rate adders with one adder operating at N times the chip rate, can be implemented both for systems having arbitrary Walsh codes and for those having Walsh codes chosen to satisfy the skinny fat finger code relationships in (1).

Interference Cancellation at the Mobile Terminal

Recently, multiuser detection via interference cancellation at the base station has been an active area of research in the CDMA community.[15-17] In general, these techniques use the knowledge of several users' codes in detecting a given desired user. The circuitry required is usually much more complex than that of a conventional single-user detector. Hence, applications of multiuser detection tend to focus on the base station receiver, which can readily handle this added complexity, rather than on the mobile terminal. Our use of multiuser detection is unusual in that it occurs at the latter, and we will demonstrate how relatively low-complexity methods can improve performance significantly over conventional detectors.

The forward link traffic channels for each mobile user are mutually orthogonal to one another and to the pilot signal. As long as multipath dispersion is present, however, there will be interference at the receiver output due to a variety of multipath components. Specifically, for a given multipath component of a desired traffic channel at the receiver, the corresponding finger's matched filter output will have unwanted contributions due to other multipath components of itself, the other channels, and the pilot signal. In the case of an MC receiver, part of these contributions amounts to self-interference among the multiple code channels it detects. The conventional rake matched filter does not account for interchannel multipath interference, and its performance can be improved if the mobile receiver takes advantage of the fact that signals from multiple codes are jointly detected.

To do so, we propose simple, yet effective, methods for *multicode self-interference suppression* that employ interference subtraction and subspace projection. The subtraction method uses existing estimates of the multipath channel parameters to reconstruct each multipath baseband pilot signal and to subtract it from the demodulator finger inputs corresponding to the other multipath components. The subspace projection method (based on the decorrelating detector[15]) makes use of the information about the N multicodes. For each of the N MC signals we wish to demodulate, the received signal is projected onto the null space of the other N–1 received multicode signal vectors. Considering their minimal implementation requirements, these methods provide significant gains in the downlink capacity of a MC-CDMA system. Note that the subtraction method applies to conventional CDMA handsets as well. In the appendix, we derive BER expressions for detectors that employ these interference suppression techniques.

Current IS-95 mobile receivers use the pilot signal to obtain amplitude and phase estimates of the channel for coherent detection. Because the relevant multipath pilot parameters (delay and complex amplitude) are already estimated by the conventional receiver and because its code is known, the pilot signal for each multipath component can be reconstructed easily and subtracted from the demodulator inputs of the other multipath components to eliminate interference. This scheme differs fundamentally from cancellation schemes that remove the interference from other data channels because the latter schemes require estimating the interferers' data bits prior to cancellation. The pilot signal is not data modulated and our subtraction scheme does not require this extra step. Thus, its

implementation is simpler and it avoids the problem of error propagation due to incorrect bit estimates.

For reference, **Figure 6** shows a block diagram of a conventional rake finger for demodulating path l ($l = 0 \ldots L-1$). The L fingers demodulate the L strongest multipath signals whose delays have been estimated using a pilot searcher. For processing the n^{th} symbol, the received signal, denoted here as $\tilde{\mathbf{r}}^{(n)}$, is an oversampled complex QPSK direct-sequence CDMA baseband signal having γ samples per chip. The on-time selector picks out every γ samples from $\tilde{\mathbf{r}}^{(n)}$ corresponding to the delay of path l. These N_c samples are collected by the on-time selector to create the chip-rate vector $\mathbf{r}_{(l)}^{(n)}$, and they are multiplied with a properly aligned short-code PN-sequence $\mathbf{p}_{(l)}^{(n)}$ to remove the pilot spreading for path l. The upper branch obtains an estimate of the current channel state, $\hat{c}_{(l)}^{(n)}$, via an accumulation over one symbol. This estimate can then be further refined in a channel-estimation algorithm (CAL) block by considering previous accumulator outputs. For example, in a slow fading channel, $\hat{c}_{(l)}^{(n)}$ may be the weighted average of the current and previous accumulator outputs. By correlating $\mathbf{r}_{(l)}^{(n)}$ with the Walsh code $\mathbf{w}_k$ of channel k, the lower branch recovers the complex amplitude of the data of path l. Multiplying by the complex conjugate of the channel estimate, the real part of the product $y_{k(l)}^{(n)}$ is delivered to a multipath combiner and then to the Viterbi decoder. The bit decision for the coded data on channel k is the hard limit of the sum of the L demodulator outputs

$$\hat{b}_k^{(n)} = \operatorname{sgn}\left(\sum_{l=0}^{L-1} y_{k(l)}^{(n)} \right).$$

We now elaborate on the interference subtraction (IS) scheme that uses the previous channel estimate to reconstruct and cancel the pilot interference from the current symbol's received signal. Because the fading rate is much slower than the symbol rate in IS-95 and the channel will not change appreciably between symbols, it is reasonable to perform cancellation using a delayed channel estimate. **Figure 7** illustrates the structure of this detector for an $L = 2$ path case. This method is recursive in that it performs subtraction

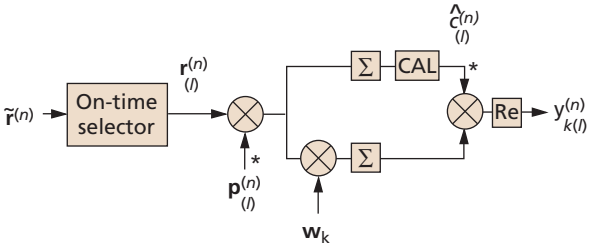

CAL – Channel estimation algorithm
Re – Real part of input (a complex number)

Figure 6.
Rake finger for the l^{th} multipath.

prior to channel estimation. Therefore, interference subtraction improves both signal demodulation and channel estimation. Without loss of generality, we focus on the relatively simple two-path signal in the figures because extending the schemes for more than two paths is straightforward. The upper reconstruction low-pass filter (RLPF) generates the samples of pilot $\mathbf{p}_{(0)}^{(n)}$ with respect to the multipath delay of path 1. These samples are weighted using the current channel estimate of path 0, $\hat{c}_{IS(0)}^{(n)}$, and subtracted from the on-time samples of path 1, $\mathbf{r}_{(1)}^{(n+1)}$, during the next symbol interval. Similarly, the pilot samples of $\mathbf{p}_{(1)}^{(n)}$ are reconstructed with respect to the multipath delay of path 0, weighted using $\hat{c}_{IS(1)}^{(n)}$ and subtracted from $\mathbf{r}_{(0)}^{(n+1)}$.

Note that the additional hardware required, shown in the shaded area of Figure 7, is minimal. The RLPF can be implemented either as a four-tap finite impulse response filter whose coefficients depend on the relative delay between the two multipath components or as a look-up table. Note also that because IS occurs prior to both channel estimation and data signal demodulation, each process benefits from the subtraction.

As with the conventional rake receiver, the L finger outputs are added to form the decision variable

$$y_{IS,k}^{(n)} \equiv \sum_{l=0}^{L-1} y_{IS,k(l)}, \qquad (2)$$

which is the input to the soft Viterbi decoder. In our performance analysis, however, we again consider the

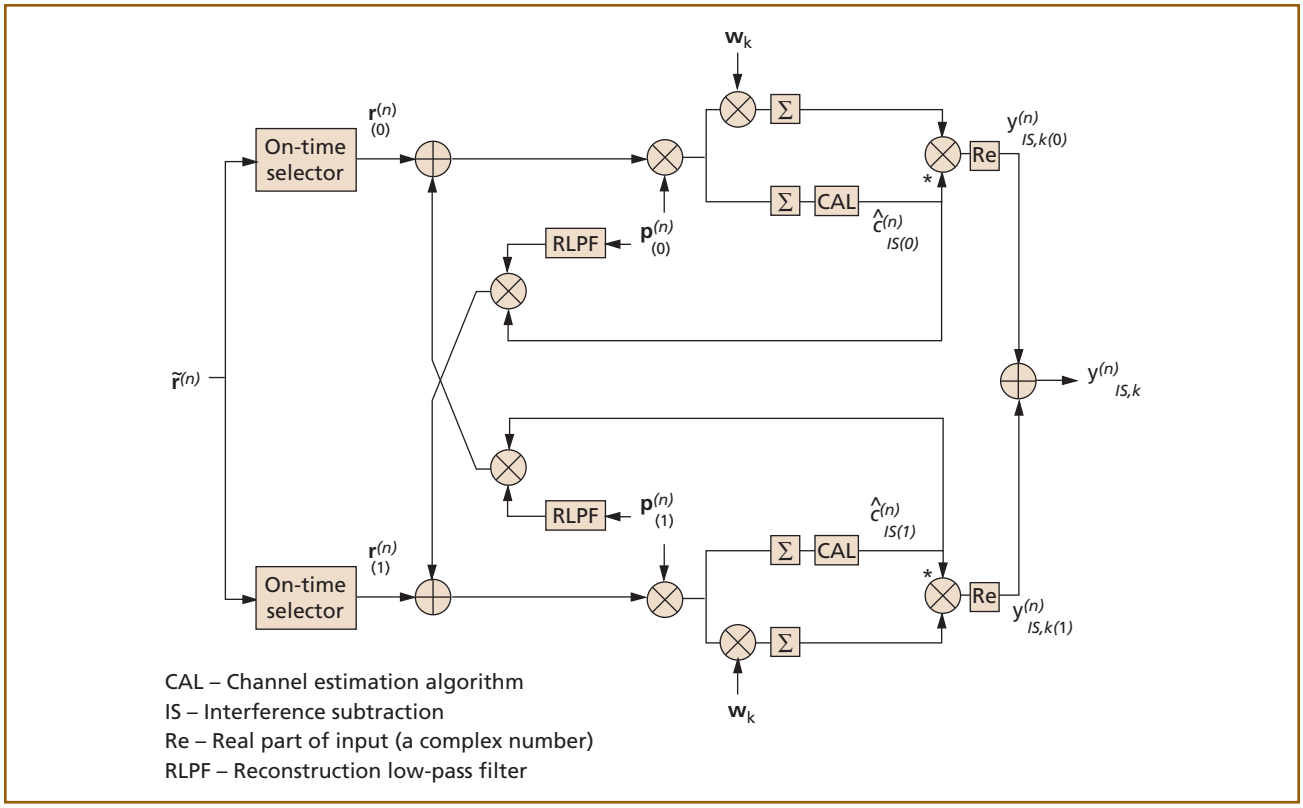

Figure 7.
Interference subtraction detector.

BER for the coded data bits based on the hard decision of the decision variable $\hat{b}^{(n)}_{IS,k} = \mathrm{sgn}\left(y^{(n)}_{\mathbf{IS},k}\right)$.

More complex IS detectors can be devised to buffer the received signals so that subtractions can be completed using channel estimates from the current symbol instead of the previous one. Such buffering methods may be attractive in extremely fast fading channels in which the channel amplitudes vary significantly from symbol to symbol. For IS-95, however—even with very fast Doppler fading (100 Hz)—the fading rate is still relatively slow compared to the bit rate (9,600 b/s), and no performance advantage is realized using the more computationally complex buffered detector. In fact, the fading is relatively slow so that the nonbuffered method, which has the advantage of interference-subtracted channel estimates for pilot reconstruction, outperforms the buffered method.

We now discuss the MC interference suppression technique via subspace projection, which is based on the decorrelating detector[16] and which we call partial decorrelation (PD). Whereas the interference suppression via subtraction applies to any mobile receiver regardless of the number of data channels it demodulates, PD applies specifically to MC receivers which demodulate $N > 1$ data channels.

Figure 8 shows the partial decorrelator for an N-code MC-CDMA receiver. The received signal is first processed by a bank of N rake-matched filters (implemented as L fat fingers) and L interference subtraction processors. The output of each enhanced rake filter, $y^{(n)}_{IS,k}$ ($k = 1...N$) given by (2), ideally will not contain pilot multipath interference in any of the N outputs. However, there will be multipath interference due to the other $N-1$ MC channels and due to the remaining $K-N$ data channels ($K \geq N$ is the total number of data channels). Using knowledge of the MC codes, the PD applies a linear transformation to the N-vector

$$\mathbf{y}^{(n)}_{IS} = \left[y^{(n)}_{IS,1} \cdots y^{(n)}_{IS,N}\right]^T$$

of rake filter outputs. Ideally, the components of the N-vector

$$\mathbf{y}^{(n)}_{IS-PD} = \left[y^{(n)}_{IS-PD,1} \cdots y^{(n)}_{IS-PD,N}\right]^T$$

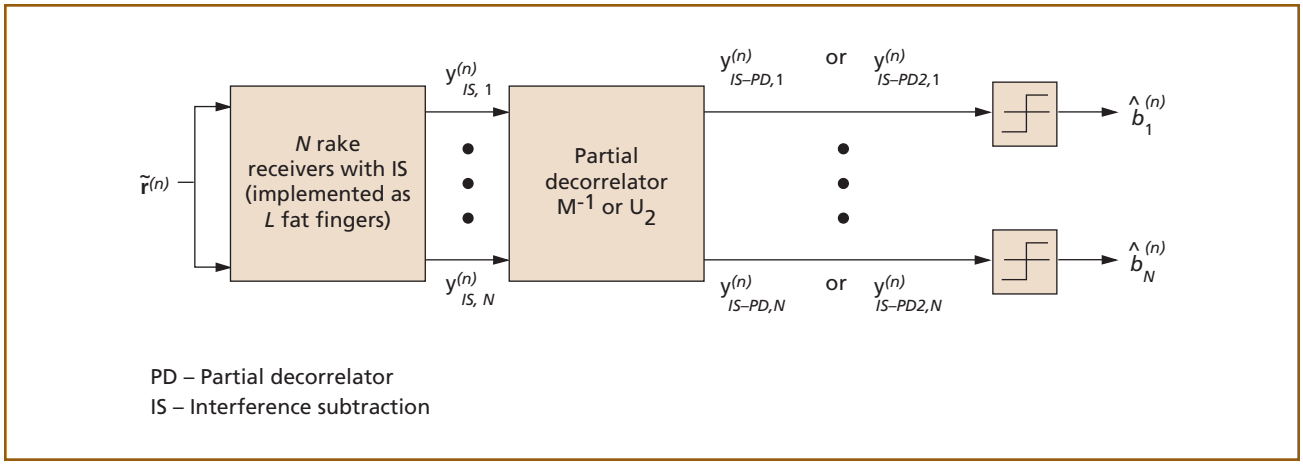

Figure 8.
Combined interference subtraction and partial decorrelating detector.

resulting from the linear transformation will be partially decorrelated from one another in that the k^{th} component will contain no interference from the $N-1$ MC channels $j = 1 \ldots N$, $j \neq k$. This component, however, may contain interference from the $K-N$ data channels not associated with this MC user. The bit decision for the k^{th} MC channel is $\hat{b}_{IS,k}^{(n)} = \text{sgn}\left(y_{IS-DD,k}\right)$.

The linear transformation is represented by the matrix inverse of the $N \times N$ correlation matrix of the MC channels $\mathbf{M}^{(n)}$; hence, the partial decorrelator output vector is $\mathbf{y}_{IS-DD}^{(n)} = \left[\mathbf{M}^{(n)}\right]^{-1} \mathbf{y}_{IS}^{(n)}$. In the absence of interference from the $K-N$ data channels, the PD is the maximum likelihood detector that has relative but not absolute knowledge of the multipath amplitudes. In practice, because the channel estimates are not perfect, the estimated correlation matrix $\mathbf{M}^{(n)}$ is not exact. Consequently, at the output of the PD, there will be residual MC interference in $\mathbf{y}_{IS-DD}^{(n)}$. In addition, there will still be some MC intersymbol interference induced by the multipath delays.

Because the channel spreading codes change between each symbol interval, the correlation matrix $\mathbf{M}^{(n)}$ and its inverse $\left[\mathbf{M}^{(n)}\right]^{-1}$ must be recomputed on each interval. Because the matrix inverse may be too computationally intensive for a mobile receiver, we are motivated to find an approximation to $\left[\mathbf{M}^{(n)}\right]^{-1}$, which is easier to calculate. An approximation based on the matrices of the diagonal and off-diagonal terms of $\mathbf{M}^{(n)}$ was analyzed for real channels.[18] As the appendix shows, a similar approximation can be made for the partial decorrelator $\left[\mathbf{M}^{(n)}\right]^{-1}$ for multipath channels. This approximation, $\mathbf{U}_2^{(n)}$, can be easily calculated using knowledge of $\mathbf{M}^{(n)}$.

The potential drawback of using the partial decorrelator to mitigate MC interference is that it can enhance background noise due to intercell interference and thermal noise.[15] In the following subsection, we show that despite the residual data channel interference and enhanced background noise, the combined IS-PD detector (and its approximation $\mathbf{U}_2^{(n)}$) provides significant performance gains over the conventional detector.

Performance analysis. This subsection discusses performance improvements of our enhanced receivers using interference cancellation over conventional detectors. The analysis applies the general result from the appendix to a specific system composed of $K = 16$ data channels with 100% voice activity. In terms of total interference, this is equivalent to a typical IS-95 system having 40 voice channels, each with 40% activity. Assuming all channels are of equal power, $A_1 = \ldots = A_{16}$, and the pilot signal is 20% of the total downlink power, the pilot amplitude A_0 is such that $A_0^2 / \left(A_0^2 + 16A_1^2\right) = 0.2$, or $A_0 = 2A_1$.

Consider a three-path Rayleigh fading channel with multipath delays of one and two chips with respect to multipath component 0. We assume the Doppler frequency is 100 Hz, which is considered the

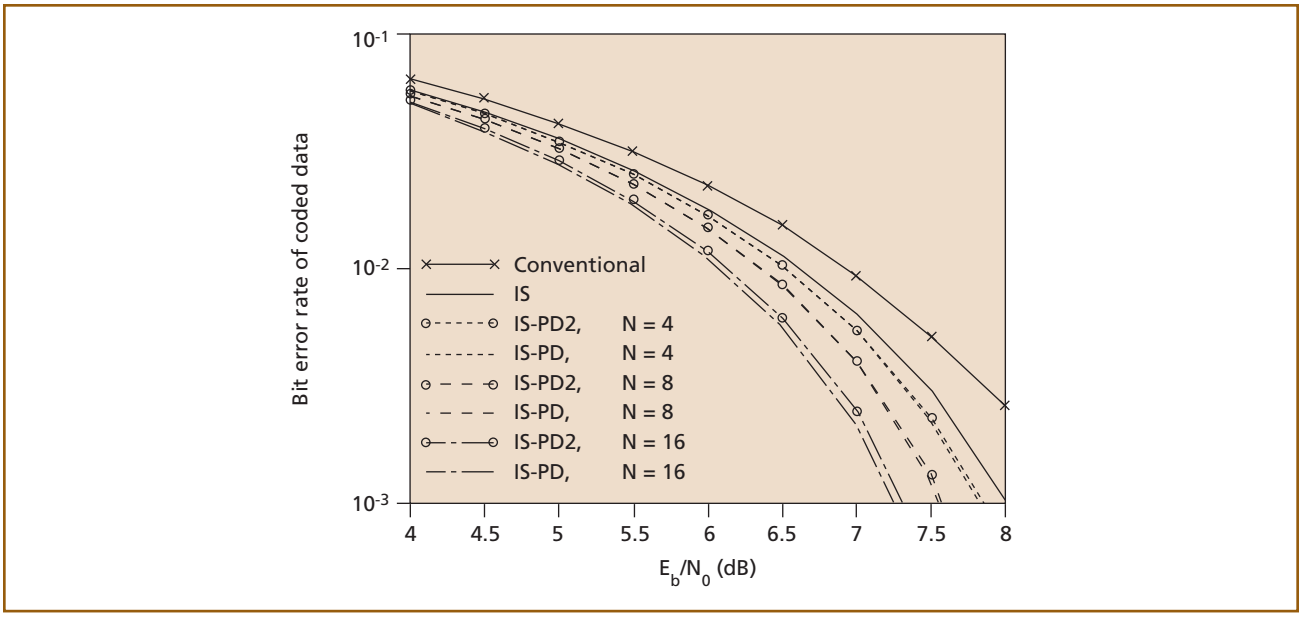

Figure 9.
Performance curves of MC-CDMA receivers with interference suppression.

worst-case fast-fading channel for IS-95. On each iteration of the simulation, we calculate the BER for a given set of random interferer bits and a given Rayleigh channel realization with noisy channel estimates. These BERs are then averaged over 10,000 iterations, and **Figure 9** shows the results. The E_b / N_0 signal-to-noise ratio (SNR) on the x-axis is defined by

$$\frac{E_b}{N_0} = \frac{A_1^2 \left(2R_c / R_b\right)}{A_0^2 + \left(K-1\right)A_1^2 + \sigma^2}, \qquad (3)$$

where σ^2 is the variance of the additive white Gaussian noise, which accounts for interference due to signals from other cells and from thermal noise and where—for IS-95—the chip-rate to bit-rate ratio R_c / R_b is 64. The top curve corresponds to the conventional receiver with no interference cancellation enhancements (see (10) in the appendix.). A BER of 3×10^{-3} (which approximately upperbounds the target 1% frame error rate) occurs at $E_b / N_0 = 7.90$ dB for the conventional detector. From (3), this requires a transmit SNR of $A_1^2 / \sigma^2 = 0.568$. The next curve corresponds to the conventional receiver with interference subtraction (see (15) in the appendix). At 3×10^{-3} BER, an improvement of 0.40 dB is indicated. Therefore, for E_b / N_0 = 7.50 dB and a fixed transmit SNR of $A_1^2 / \sigma^2 = 0.588$, (3) gives K = 18.0. Consequently, at 3×10^{-3} BER, the IS detector increases the downlink capacity by 12.5% over the conventional detector.

The next two curves shows the BER for one data channel of an N = 4 MC receiver that uses the combined IS and, respectively, the partial decorrelator $\left[\mathbf{M}^{(n)}\right]^{-1}$ (see (23) in the appendix) and approximate partial decorrelator $\mathbf{U}_2^{(n)}$ (27). Except at high SNR, there is no noticeable performance loss in using the more easily calculated approximate PD. Despite the fact that the decorrelation occurs for only one quarter of the 16 data channels, a noticeable performance improvement still results. The required E_b / N_0 for 3×10^{-3} BER drops another 0.15 dB to 7.35 dB, and the IS-PD provides a 17.5% increase in downlink capacity over the conventional detector. For N = 8, partial decorrelation accounts for the MC interference due to half the data channels. At 3×10^{-3} BER, there is a 0.78 dB performance gain over the conventional detector, and like the case of N = 4, there is negligible performance loss in using the approximate PD. Finally, if all 16 data channels are demodulated by a single MC user, the performance gains are tremendous if the PD $\left[\mathbf{M}^{(n)}\right]^{-1}$ is used. In such a case, however, the required 16×16 matrix inversion for computing $\left[\mathbf{M}^{(n)}\right]^{-1}$ is costly. Alternatively, most of the perfor-

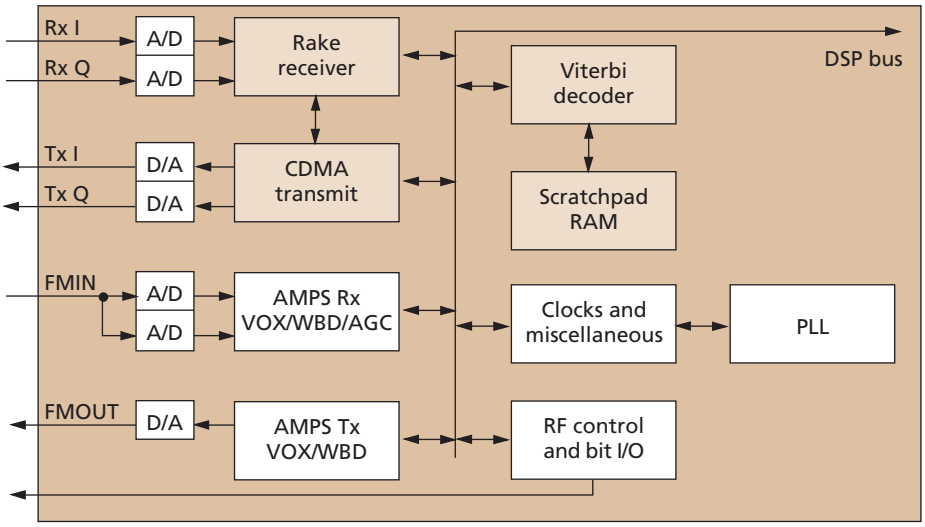

A/D – Analog to digital
AGC – Automatic gain control
AMPS – Advanced Mobile Phone Service
CDMA – Code division multiple access
D/A – Digital to analog
DSP – Digital signal processor
FM – Frequency modulation
PLL – Phase lock loop
RAM – Random access memory
RF – Radio frequency
VOX – Voice
WBD – Wideband data

Figure 10.
Typical dual-mode IS-95 baseband ASIC.

mance gains can be achieved using the approximation $\mathbf{U}_2^{(n)}$.

Recall that each data channel is received with the same power. A common misconception of multiuser detectors is that they provide performance improvements only in near-far environments in which the received power of a desired channel is lower than that of the interferers. However, our results show that even in environments having perfect power control, multiuser detection techniques such as those proposed in this section can provide significant performance gains over conventional detectors with minimal added complexity. The performance improvement of the IS and PD interference suppression techniques increases with E_b / N_0 because of improved channel estimates. Thus, applications that demand low BERs and high SNRs gain the most.

MC-CDMA Handset ASIC at 56 kb/s

This section discusses the impact of MC-CDMA on a typical IS-95 CDMA mobile terminal. Base station hardware requires only minimal changes when upgrading to MC-CDMA specifications. Unfortunately, this is not the case for the mobile station. Base stations already support multiple (up to 64) code channels per carrier but existing handsets support only one. Our basis for comparison is a typical IS-95 physical-layer application-specific integrated circuit (ASIC) that implements the baseband portions of the IS-95 CDMA physical layer in conjunction with a digital signal processor (DSP).

To support a 56-kb/s rate, we must implement MC-CDMA with $N = 4$ to quadruple the basic IS-95 rate (14.4 kb/s). As a first approximation, it might be expected that this will quadruple the number of gates in the ASIC. We determined, however, that it is possible to achieve significant sharing among functions. In some areas, we find that simply increasing clock speed boosts throughput. Additionally, power consumption of the ASIC scales in direct proportion to the data rate when implementing the modifications we propose. As a result, operation at the basic rate does not

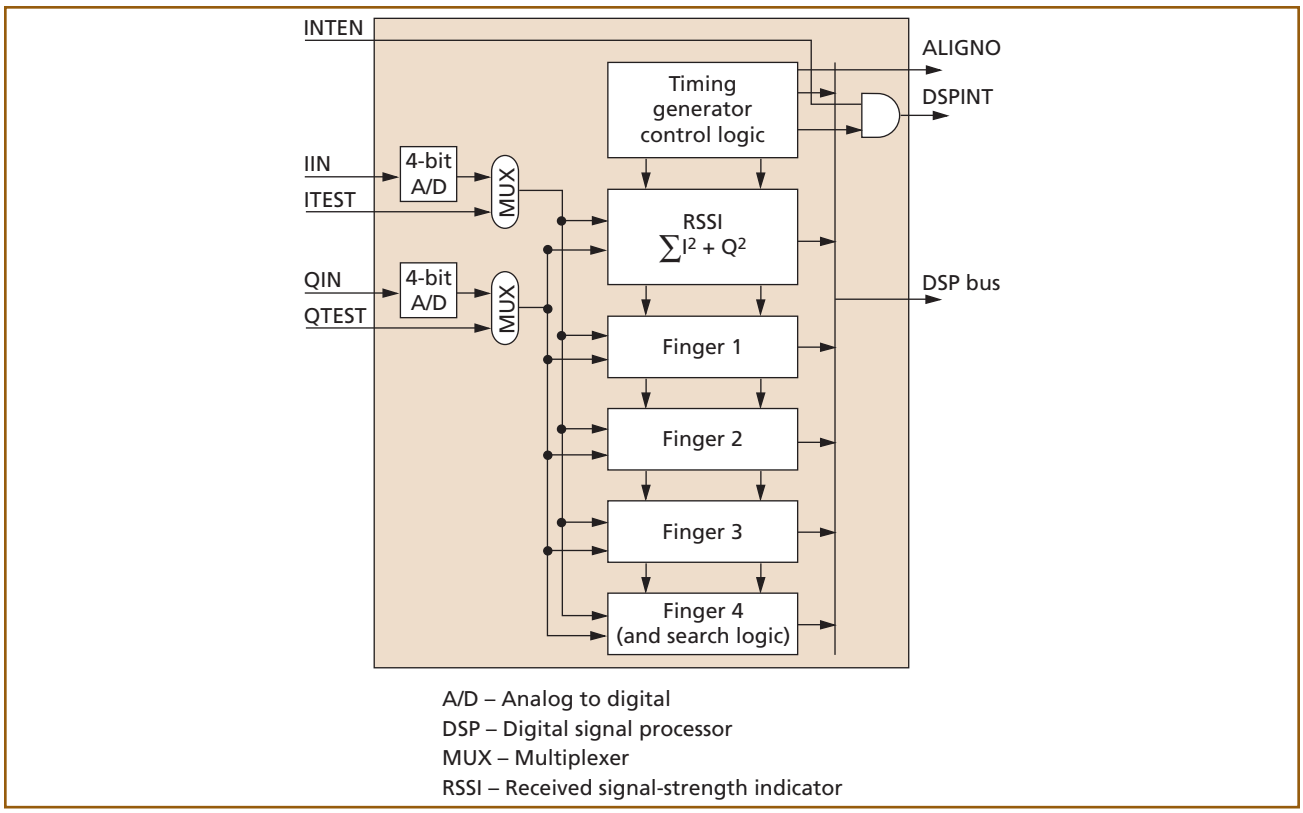

Figure 11.
Typical rake receiver.

require significantly more power than the existing ASIC design. Based on our estimates, adding MC-CDMA ($N = 4$) support to the ASIC will increase the gate count by only 55%—significantly less than the anticipated factor of four.

Figure 10 is a block diagram of a typical dual-mode IS-95 ASIC. The ASIC comprises approximately 70,000 digital logic gates, a 2,000-word static random access memory (SRAM), and several analog-to-digital converter cells. Blocks requiring changes for MC-CDMA are shaded.

The three subsections that follow discuss each main functional block affected by the changes: the rake receiver, Viterbi decoder, and CDMA transmitter. Each subsection discusses the impact of the changes, suggests alternatives, and estimates the increase in gate count.

Rake Receiver

To take advantage of the inherent diversity in a multipath environment, CDMA receivers typically use a structure known as a *rake*, which has several mostly identical fingers. Each finger de-spreads and demodulates a single multipath component of the received signal.

Figure 11 shows a typical four-finger rake receiver for a mobile terminal. In addition to the fingers, this rake receiver has a microprocessor interface, a common timing generator, and a received signal-strength indicator (RSSI). One finger, which is used as a high-speed pilot searcher, has a small amount of extra logic. The RSSI block calculates an estimate of total received power, which is used for automatic gain control (AGC) and reverse-link power control.

For the MC-CDMA forward link, all Walsh channels received on a single multipath component arrive simultaneously so that a single finger tracking a given pilot acquires the necessary timing to de-spread all the Walsh channels. Therefore, the problem of pilot tracking and acquisition is not exacerbated by having to demodulate multiple Walsh channels. As a result, the changes needed for MC-CDMA are confined to the three identical data fingers while the search finger,

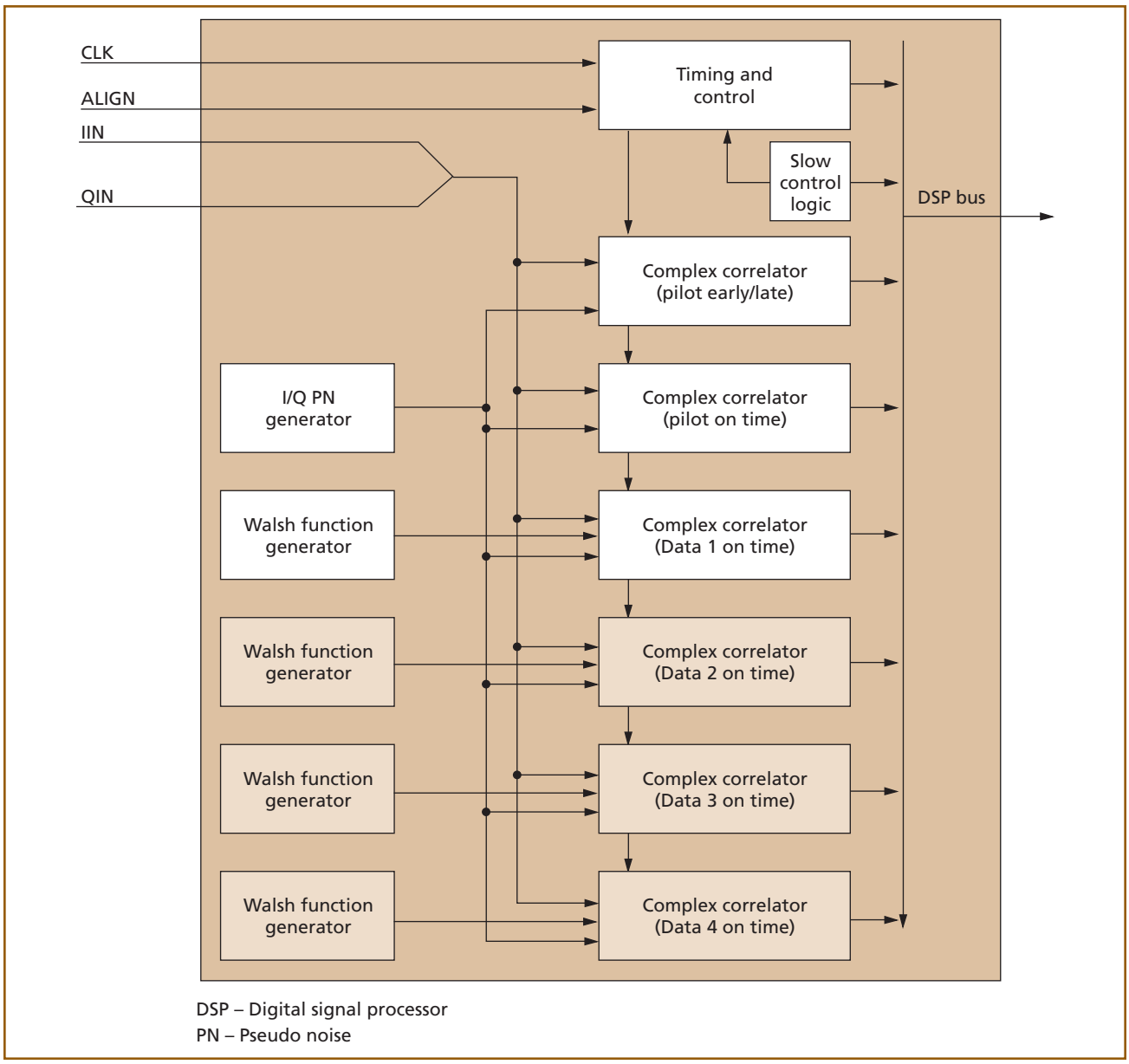

Figure 12.
Fat finger architecture for coherent MC-CDMA with N = 4.

RSSI block, and much of the common logic require no modifications.

Figure 12 illustrates a rake finger as modified for MC-CDMA. The unshaded blocks represent the parts of a rake finger needed to receive and de-spread a single Walsh channel. It includes three complex correlators: one for pilot on-time, one for pilot early/late, and one for data on-time. The DSP performs optimum combining using the output of the data and pilot on-time correlators from each finger. It also compares the output of the pilot on-time and pilot early/late correlators for pilot tracking and automatic frequency control (AFC). For MC-CDMA having N simultaneous Walsh channels for a single receiver, $N - 1$ complex correlators must be added to each finger, one for each additional Walsh channel. Thus, the shaded blocks in Figure 12 show the additional logic required for the case of $N = 4$.

This logic is contained entirely within the fingers of the rake receiver, and the fingers are similar

to a single channel finger (but larger). Therefore, we call this structure a fat finger. In fact, the fat finger differs from a regular finger only in the number of data on-time correlators. By sharing the pilot correlators, the fat finger saves *2(N–1)* complex correlators for an MC-CDMA system supporting *N* times the basic rate. In addition, further enhancements[20] are possible, such as the skinny fat finger described earlier. The savings in the number of required complex correlators reduce the number of operations needed for such a receiver and translate directly into power savings for the mobile terminal.

The digital logic for the rake receiver requires about 30,000 gates. Breaking this number down into components, we find that a finger is 6,000 gates and a complex correlator (within a finger) is 1,800 gates. For MC-CDMA ($N = 4$), we must add nine complex correlators (three per finger for three fingers), totaling 16,200 gates, which we round up to 20,000 gates. Thus, a rake receiver for MC-CDMA can be implemented with about 50,000 gates, a 60% increase over a conventional IS-95 CDMA receiver.

Viterbi Decoder

Both the forward and reverse links of the IS-95 CDMA system employ a convolutional encoding scheme for error protection. Using received channel symbols, the Viterbi decoder traces a path through the state trellis to determine the nearest possible correct path and reconstructs the original bit stream from this path. The algorithm evaluates all possible states at each point in time so that if 2^{C-1} possible states and M symbols per frame are available, the complexity of the algorithm is $O(M\,2^{C-1})$.

The variable C is called the constraint length, and it is determined by the order of the polynomial used in the convolutional encoder. For IS-95, the constraint length is 9, and a 20-ms frame has 384 symbols.

The complexity of the Viterbi decoding process and the high throughput requirements dictate that the decoder in existing mobile terminals be implemented in custom hardware. However, improvements in DSPs soon may enable a software implementation of the Viterbi algorithm, obviating the need for specialized hardware.

In a typical IS-95 ASIC, the Viterbi decoder is implemented as a coprocessor to the DSP, taking a frame of symbols from the DSP and returning the decoded bits. The decoder comprises 10,000 gates of logic and a 2,000-word SRAM. Assuming a 20-MHz system clock, it takes approximately 10 ms to decode a full-rate 20-ms data frame.

One approach to increasing the speed of a Viterbi decoder is simply to increase its clock frequency within the inherent constraint of the chosen ASIC technology. Because it is reasonable to expect that current ASIC technologies can support operation at 40 MHz, which is two times the typical clock speed—we can easily achieve an improvement factor of two in throughput.

The remaining bottleneck in the decoding process is the evaluation of the path metrics for each state in the trellis. Due to similarities between the Viterbi algorithm and the computation of the fast Fourier transform, some common techniques[19] can be employed using minimal additional hardware to alleviate this bottleneck and further double the decoder throughput. Specifically, this process requires the addition of a second path metric processor and replacement of a small part of the scratch pad RAM with a 256-word dual-port memory. The additional path metric processor requires about 2,000 gates, so the increase in both logic and memory is about 20%.

Figure 13 illustrates a possible implementation of the Viterbi decoder with the above enhancements. Note that the number of operations it performs is directly related to the amount of data processed, so the power dissipation scales similarly.

MC-CDMA Reverse-Link Transmitter

Typically, the final digital stages of an IS-95 CDMA transmitter from Walsh modulation through digital-to-analog conversion are implemented as part of the ASIC. Conceptually, this represents all subsymbol operations following the interleaver. **Figure 14** shows a possible implementation of a transmitter for the MC-CDMA reverse link with subcode concatenation. Support for MC-CDMA with $N = 4$ requires the addition of three Walsh modulators, three direct sequence spreaders, and three quadrature spreaders. These modifications are straightforward and relatively minor. If the reverse link uses subcode con-

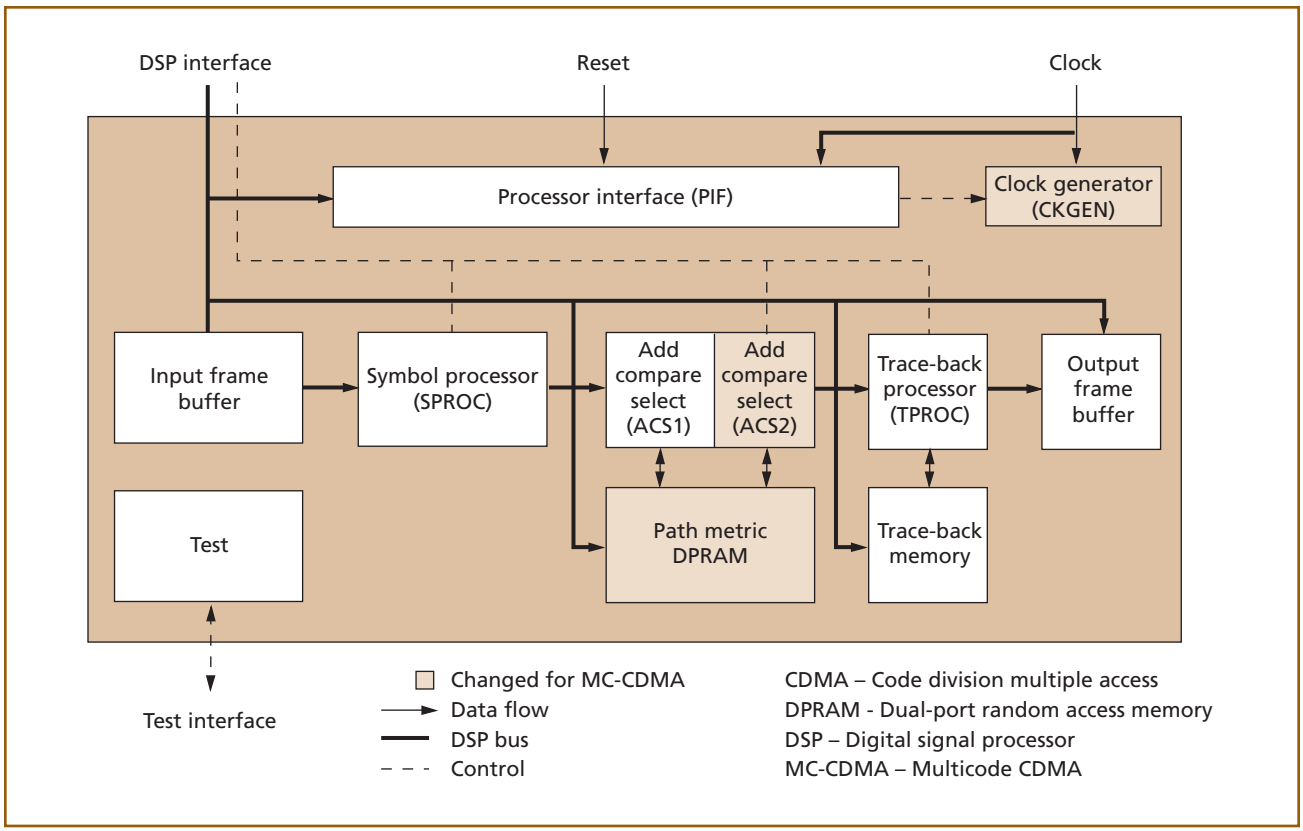

Figure 13.
MC-CDMA Viterbi decoder.

catenation, then we must also add a subcode generator (shown in Figure 3). If the reverse link uses code aggregation, then three additional long PN code generator masks are needed. The net effect of both these additions is relatively minor because the operations involved (2-bit counter and/or several *xor* gates) are comparatively simple. The bulk of the logic for the transmitter is found in the I and Q FIR filters, which are discussed next.

Figure 15 illustrates a possible implementation of an FIR filter for an MC-CDMA system. For typical IS-95 CDMA ASICs, the input to each transmit FIR is a 2-bit signal that permits multiplier-less implementation. This is a significant hardware optimization that should be preserved in enhanced implementations. One bit of the 2-bit filter input is the transmitted data and the other bit is a control signal that enables or disables transmission of data. The effect of this control signal is to allow smooth transitions between the active and idle states for each channel as required to comply with IS-95 standards. For MC-CDMA, however, four 2-bit inputs to the FIR must be added. Because the FIR filter is a linear operation, we can perform the addition of these signals either before or after the filter. By choosing to filter each channel independently and adding the results afterward, we maintain the advantage of the simple multiplier-less structure for the MC-CDMA implementation. We then quadruple the FIR throughput by increasing the clock speed, which is reasonable because the frequencies involved are relatively low. We can further improve this scheme by scaling the clock frequency based on the instantaneous data rate so that the power dissipation of the filter is directly proportional the amount of data transmitted.

A typical CDMA transmitter requires approximately 25,000 gates with the majority in the FIR filters. For MC-CDMA, 5,000 gates must be added to the FIR filters and 2,000 gates must be added for the Walsh modulators, subcode generators, and other logic. The net addition to the transmitter is about 7,000 gates, an increase of only 28%.

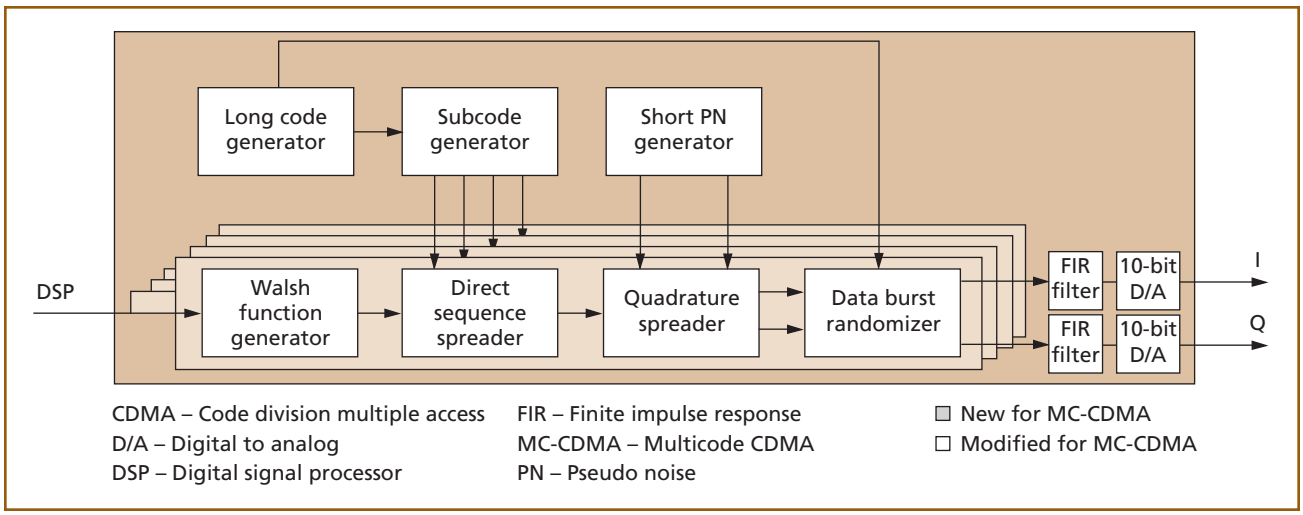

Figure 14.
MC-CDMA reverse-link transmitter (N = 4).

ASIC Modifications

In our discussion of the impact of MC-CDMA on the design of a mobile terminal, we mentioned power dissipation issues only briefly and focused instead on the increase in logic complexity. While the power dissipation of an MC-CDMA mobile terminal clearly will be greater than that of a conventional terminal, it will not increase in direct proportion to the data rate because much of the fixed overhead remains the same for both. Moreover, we have attempted to minimize the increase wherever possible as discussed in the earlier "Rake Receiver," "Viterbi Decoder," and "MC-CDMA Reverse-Link Transmitter" subsections.

Modifications to the digital logic required to support MC-CDMA ($N = 4$) represent an increase of about 30,000 gates and the addition of a small dual-port RAM. This is an increase of less than 55% compared to a single-channel IS-95 ASIC, and it results in a relatively small increase in hardware complexity for such a significant extension of data-rate capability.

DSP and RF Implications

DSP processing is not as important an issue at the base station as it is at the mobile terminal because it is not as constrained in terms of power and size. We expect that roughly 25% more DSP processing would be required at the mobile terminal to support MC-CDMA with $N = 4$ times the basic rate. This increase is relatively small because many of the physical-layer algorithms for IS-95 CDMA—for example, timing acquisition, AGC, and AFC, are unchanged for MC-CDMA. As for the RF section, little if any change is required at the base station whereas the linearity of the mobile terminal power amplifier must be improved by 2.7 dB.

Conclusion

As part of an effort to provide multimedia services to CDMA cellular and PCS users, MC-CDMA provides a logical extension to existing IS-95 systems. It bridges the gap between today's standards and future service needs through a simple enhancement of the current architecture, requiring little or no change to existing hardware.

At the system level, true multimedia services require bandwidth-on-demand access control. The LIDA access control mechanism allows dynamic rate allocation for mixed traffic in a cellular CDMA environment. LIDA builds on existing pilot-measurement and soft hand-off protocols, and it can be integrated easily with IS-95.

At the physical layer of the mobile tranceiver, to minimize receiver complexity in terms of hardware cost, power consumption, and design effort, we presented three fat finger enhancements of the rake receiver exploit the inherent timing and synchronization characteristics available in all MC-CDMA systems. Interference suppression techniques presented here were shown to increase downlink capacity by 17.5%

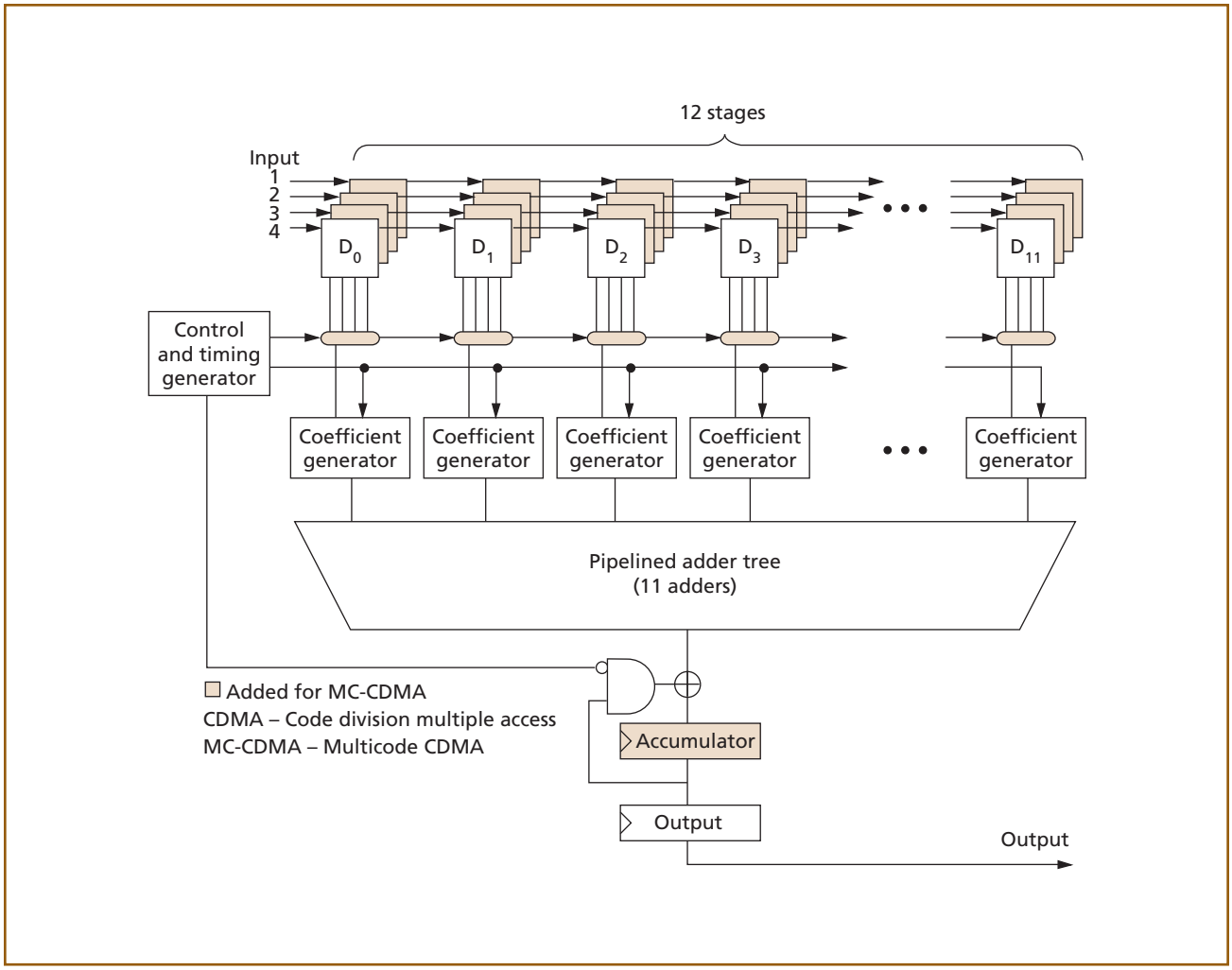

Figure 15.
MC-CDMA reverse-link transmit FIR (N = 4).

for a $N = 4$ multicode system at 3×10^{-3} BER. Applications demanding low BERs gain the most from such techniques. Finally, we presented an efficient implementation of a 56-kb/s MC-CDMA mobile transceiver design with minimal complexity and hardware costs.

MC-CDMA is readily applicable to existing IS-95 systems. In conjunction with the LIDA access control scheme, interference suppression, and fat finger mobile receiver, MC-CDMA provides a simple and effective transition to future high-speed wireless services.

Appendix. Performance Analysis of IS-95 Detectors with Interference Cancellation

We derive analytic expressions for the bit error rates of the conventional detector, the interference subtraction detector, and the combined interference subtraction and partial decorrelating detector. Numerical results based on these analytic expressions are presented in the "Performance Analysis" subsection.

Definitions

Consider an L multipath downlink signal, which contains the pilot signal and K traffic/sync channels. Subchip rate samples of the complex baseband received signal are obtained by sampling at a rate of γ

samples per chip interval. We assume that the channel amplitude remains constant over a symbol interval but that it can vary from symbol to symbol. Likewise, IS-95 dictates that the pilot and data channel codes (which are component-wise products of Walsh sequences and the short code sequence) vary from symbol to symbol. During bit interval n, the receiver processes $\gamma N_c + \delta_{L-1}$ complex-valued samples, where N_c is the number of chips per symbol and δ_l is the delay of multipath signal l ($l = 0 \ldots L-1$) in terms of integer subchip intervals. Without loss of generality, we order the delays such that $\delta_{L-1} > \delta_{L-2} > \ldots > \delta_0 = 0$. The received samples are collected to form a complex $(\gamma N_c + \delta_{L-1})$ -vector $\tilde{\mathbf{r}}^{(n)}$

$$\begin{aligned}\tilde{\mathbf{r}}^{(n)} = &\sum_{l=0}^{L-1} c_{(l)}^{(n)} \left[A_0 \tilde{\mathbf{p}}_{(l)}^{(n)} + \sum_{k=1}^{K} A_k \tilde{\mathbf{s}}_{k(l)}^{(n)} b_k^{(n)} \right] \\ &+ \sum_{l=1}^{L-1} c_{(l)}^{(n-1)} \left[A_0 \tilde{\mathbf{p}}_{(l)}^{(n-1)}[\mathrm{L}] + \sum_{k=1}^{K} A_k \tilde{\mathbf{s}}_{k(l)}^{(n-1)}[\mathrm{L}] b_k^{(n-1)} \right] \quad (4) \\ &+ \sum_{l=0}^{L-2} c_{(l)}^{(n+1)} \left[A_0 \tilde{\mathbf{p}}_{(l)}^{(n+1)}[\mathrm{R}] + \sum_{k=1}^{K} A_k \tilde{\mathbf{s}}_{k(l)}^{(n+1)}[\mathrm{R}] b_k^{(n+1)} \right] \\ &+ \tilde{\mathbf{n}}^{(\mathbf{n})},\end{aligned}$$

where $c_{(l)}^{(n)}$ is the complex channel amplitude of multipath signal l during symbol n; A_0 and A_k, respectively, are the real amplitudes of the pilot signal and data signal k; $b_k^{(n)}$ is the data bit of channel k during symbol n (in our bit error rate analysis, we assume without loss of generality that the bit value of the desired user k is one: $b_k^{(n)} = 1$.); $\tilde{\mathbf{n}}^{(n)}$ is complex zero-mean additive white noise vector whose real and imaginary components are i.i.d. with covariance $\sigma^2 \mathbf{I}_{\gamma N_c + \delta_{L-1}}$, where $\mathbf{I}_q$ is a $q \times q$ identity matrix and σ^2 is the noise variance as defined in (3); $\tilde{\mathbf{p}}_{(l)}^{(n)}$ and $\tilde{\mathbf{s}}_{k(l)}^{(n)}$ ($l = 0 \ldots L-1$), respectively, are the complex pilot subchip-rate spreading code and the k^{th} data channel subchip-rate spreading code of multipath signal l during symbol n. These $(\gamma N_c + \delta_{L-1})$ -vectors are padded with zeros so that their nonzero signal components are appropriately aligned to the corresponding multipath delay. In other words, for $\tilde{\mathbf{p}}_{(l)}^{(n)}$ and $\tilde{\mathbf{s}}_{k(l)}^{(n)}$, the first δ_l elements are zero, followed by the γN_c nonzero subchip-rate signal components corresponding to multipath l, followed by $\delta_{L-1} - \delta_l$ zeros. The remaining terms in (4) correspond to the intersymbol interference caused by signals on symbol intervals ($n - 1$) and ($n + 1$). Specifically, the first δ_l elements of $\tilde{\mathbf{p}}_{(l)}^{(n-1)}[\mathrm{L}]$ and $\tilde{\mathbf{s}}_{k(l)}^{(n-1)}[\mathrm{L}]$ ($l = 1 \ldots L-1$; the "L" in brackets denotes the "left"-side interference) are the last δ_l nonzero elements of $\tilde{\mathbf{p}}_{(l)}^{(n-1)}$ and $\tilde{\mathbf{s}}_{k(l)}^{(n-1)}$, respectively, and the remaining elements are all zero. Similarly, the last $\delta_{L-1} - \delta_l$ elements of $\tilde{\mathbf{p}}_{(l)}^{(n-1)}[\mathrm{R}]$ and $\tilde{\mathbf{s}}_{k(l)}^{(n-1)}[\mathrm{R}]$ ($l = 0 \ldots L-2$; "R" in brackets denotes the "right"-side interference) are the first $\delta_{L-1} - \delta_l$ nonzero elements of $\tilde{\mathbf{p}}_{(l)}^{(n+1)}$ and $\tilde{\mathbf{s}}_{k(l)}^{(n+1)}$, respectively, and the remaining elements are all zero.

Let $\mathbf{r}_{(l)}^{(n)}$ be the chip-rate output of the l^{th} on-time selector. In other words, it is an N_c-vector containing elements $\delta_l, \delta_l + \gamma, \ldots, \delta_l + (N_c - 1)\gamma$ of $\tilde{\mathbf{r}}^{(n)}$ whose elements are numbered 0, 1, ..., $\gamma N_c + \delta_{L-1} - 1$. Thus,

$$\begin{aligned}\mathbf{r}_{(l)}^{(n)} = &\sum_{j=0}^{L-1} c_{(j)}^{(n)} \left[A_0 \mathbf{p}_{(j[l])}^{(n)} + \sum_{k=1}^{K} A_k \mathbf{s}_{k(j[l])}^{(n)} b_k^{(n)} \right] \\ &+ \sum_{j=1}^{L-1} c_{(j)}^{(n-1)} \left[A_0 \mathbf{p}_{(j[l])}^{(n-1)}[\mathrm{L}] + \sum_{k=1}^{K} A_k \mathbf{s}_{k(j[l])}^{(n-1)}[\mathrm{L}] b_k^{(n-1)} \right] \quad (5) \\ &+ \sum_{j=0}^{L-2} c_{(j)}^{(n+1)} \left[A_0 \mathbf{p}_{(j[l])}^{(n+1)}[\mathrm{R}] + \sum_{k=1}^{K} A_k \mathbf{s}_{k(j[l])}^{(n+1)}[\mathrm{R}] b_k^{(n+1)} \right] \\ &+ \mathbf{n}^{(\mathbf{n})},\end{aligned}$$

where $\mathbf{p}_{(j[l])}^{(n)}$ is defined as the N_c-vector whose elements are those of $\tilde{\mathbf{p}}_{(j)}^{(n)}$ corresponding to the output of the on-time selector for multipath l. Hence, $\mathbf{p}_{(j[l])}^{(n)}$ contains elements $\delta_l, \delta_l + \gamma, \ldots, \delta_l + (N_c - 1)\gamma$ of $\tilde{\mathbf{p}}_{(j)}^{(n)}$, and we use $\mathbf{p}_{(j)}^{(n)}$ as shorthand for $\mathbf{p}_{(j[j])}^{(n)}$. We also define the analogous N_c-vectors $\mathbf{p}_{(j[l])}^{(n+1)}[\mathrm{L/R}]$ as the N_c-vector whose elements are those of $\tilde{\mathbf{p}}_{(j)}^{(n\pm1)}[\mathrm{L/R}]$ corresponding to the output of the on-time selector for multipath j. Similarly, $\mathbf{s}_{k(j[l])}^{(n)}$, $\mathbf{s}_{k(j)}^{(n)}$, and $\mathbf{s}_{k(j[l])}^{(n\pm1)}[\mathrm{L/R}]$ denote the analo-

gous chip-rate N_c-vectors for the data channel spreading codes. The on-time spreading code sample vector $\mathbf{s}_{k(j)}^{(n)}$ is the component-wise product of the corresponding pilot vector $\mathbf{p}_{(j)}^{(n)}$ and the N_c-length Walsh code vector of channel k ($\mathbf{w}_k$): $\mathbf{s}_{k(j)}^{(n)} = \mathbf{p}_{(l)}^{(n)} \circ \mathbf{w}_k$ .These chip-rate spreading code vectors are normalized such that $\left\langle \mathbf{s}_{k(j)}^{(n)}, \mathbf{s}_{k(j)}^{(n)} \right\rangle = \left\langle \mathbf{p}_{(j)}^{(n)}, \mathbf{p}_{(j)}^{(n)} \right\rangle = 1$, where $\langle \mathbf{x}, \mathbf{y} \rangle$ denotes the inner product between complex vectors $\mathbf{x}$ and $\mathbf{y}$.

Conventional Detector

Using the conventional detector, the output of the pilot correlator's l^{th} finger accumulator is $\left\langle \mathbf{p}_{(l)}^{(n)}, \mathbf{r}_{(l)}^{(n)} \right\rangle$. To simplify the analysis, we assume that the channel estimation algorithm block in Figure 10 uses only the current accumulator output for the channel estimate. Therefore, the channel estimate is the accumulator output normalized by the pilot amplitude

$$\hat{c}_{(l)}^{(n)} = \frac{1}{A_0} \left\langle \mathbf{p}_{(l)}^{(n)}, \mathbf{r}_{(l)}^{(n)} \right\rangle.$$

Note that in the actual implementation, normalization is not necessary. We use it in the analysis, however, so that if the channel estimates are perfect (that is, there is no background noise and no multipath interference), we have $\hat{c}_{(l)}^{(n)} = c_{(l)}^{(n)}$. The output of demodulator finger l for channel k is the correlation of the received signal and the k^{th} spreading code weighted by the conjugate of the l^{th} channel estimate

$$y_{k(l)}^{(n)} = \hat{c}_{(l)}^{(n)*} \left\langle \mathbf{s}_{k(l)}^{(n)}, \mathbf{r}_{(l)}^{(n)} \right\rangle. \tag{6}$$

We now introduce some matrix notation that will allow us to write explicit expressions for the channel estimates and demodulator finger outputs. Let $\mathbf{R}_{[j,k]}^{(n)}$ be the $L \times L$ correlation matrix among the L paths of data channels j and k—that is, element (u, v) of $\mathbf{R}_{[j,k]}^{(n)}$ is $\left\langle \mathbf{s}_{j(u)}^{(n)}, \mathbf{s}_{k(v[u])}^{(n)} \right\rangle$. Let $\mathbf{R}_{[P,k]}^{(n)}$ be the $L \times L$ correlation matrix among the multipaths of the pilot signal and of the data channel k—that is, element (u, v) of $\mathbf{R}_{[P,k]}^{(n)}$ is $\left\langle \mathbf{p}_{(u)}^{(n)}, \mathbf{s}_{k(v[u])}^{(n)} \right\rangle$. Similarly, element (u, v) of $\mathbf{R}_{[k,P]}^{(n)}$ is $\left\langle \mathbf{s}_{k(u)}^{(n)}, \mathbf{p}_{(v[u])}^{(n)} \right\rangle$, and element (u, v) of $\mathbf{R}_{[P,P]}^{(n)}$ is $\left\langle \mathbf{p}_{(u)}^{(n)}, \mathbf{p}_{(v)}^{(n)} \right\rangle$. Analogous matrices are defined to denote the correlations between the signals during symbols n and $n \pm 1$ as follows: element (u, v) of $\mathbf{R}_{[j,k]}^{(n\pm1)}$ is $\left\langle \mathbf{s}_{j(u)}^{(n)}, \mathbf{s}_{k(v[u])}^{(n\pm1)}[\mathrm{L/R}] \right\rangle$; element (u, v) of $\mathbf{R}_{[P,k]}^{(n\pm1)}$ is $\left\langle \mathbf{p}_{(u)}^{(n)}, \mathbf{s}_{k(v[u])}^{(n\pm1)}[\mathrm{L/R}] \right\rangle$; element (u,v) of $\mathbf{R}_{[k,P]}^{(n\pm1)}$ is $\left\langle \mathbf{s}_{k(u)}^{(n)}, \mathbf{p}_{(v[u])}^{(n\pm1)}[\mathrm{L/R}] \right\rangle$; and element (u, v) of $\mathbf{R}_{[P,P]}^{(n\pm1)}$ is $\left\langle \mathbf{p}_{(u)}^{(n)}, \mathbf{p}_{(v[u])}^{(n\pm1)}[\mathrm{L/R}] \right\rangle$. Finally, we define the following $L \times (K + 1)$ L matrices:

$$\mathbf{R}_k^{(n)} \equiv \left[\mathbf{R}_{[k,P]}^{(n)} \mathbf{R}_{[k,1]}^{(n)} \cdots \mathbf{R}_{[k,K]}^{(n)} \right]$$
$$\mathbf{R}_k^{(n-1)} \equiv \left[\mathbf{R}_{[k,P]}^{(n-1)} \mathbf{R}_{[k,1]}^{(n-1)} \cdots \mathbf{R}_{[k,K]}^{(n-1)} \right]$$
$$\mathbf{R}_k^{(n+1)} \equiv \left[\mathbf{R}_{[k,P]}^{(n+1)} \mathbf{R}_{[k,1]}^{(n+1)} \cdots \mathbf{R}_{[k,K]}^{(n+1)} \right]$$
$$\mathbf{R}_P^{(n)} \equiv \left[\mathbf{R}_{[P,P]}^{(n)} \mathbf{R}_{[P,1]}^{(n)} \cdots \mathbf{R}_{[P,K]}^{(n)} \right]$$
$$\mathbf{R}_P^{(n-1)} \equiv \left[\mathbf{R}_{[P,P]}^{(n-1)} \mathbf{R}_{[P,1]}^{(n-1)} \cdots \mathbf{R}_{[P,K]}^{(n-1)} \right]$$
$$\mathbf{R}_P^{(n+1)} \equiv \left[\mathbf{R}_{[P,P]}^{(n+1)} \mathbf{R}_{[P,1]}^{(n+1)} \cdots \mathbf{R}_{[P,K]}^{(n+1)} \right].$$

Using these definitions, we can write the collection of L channel estimates as

$$\hat{\mathbf{c}}^{(n)} \equiv \begin{bmatrix} \hat{c}_{(0)}^{(n)} \\ \vdots \\ \hat{c}_{(L-1)}^{(n)} \end{bmatrix} = \frac{1}{A_0} \begin{bmatrix} \left\langle \mathbf{p}_{(0)}^{(n)}, \mathbf{r}_{(0)}^{(n)} \right\rangle \\ \vdots \\ \left\langle \mathbf{p}_{(L-1)}^{(n)}, \mathbf{r}_{(L-1)}^{(n)} \right\rangle \end{bmatrix}$$
$$= \frac{1}{A_0} \left\{ \mathbf{R}_P^{(n)} \mathbf{C}^{(n)} \mathbf{A} \begin{bmatrix} 1 \\ \mathbf{b}^{(n)} \end{bmatrix} + \mathbf{R}_P^{(n-1)} \mathbf{C}^{(n-1)} \mathbf{A} \begin{bmatrix} 1 \\ \mathbf{b}^{(n-1)} \end{bmatrix} + \mathbf{R}_P^{(n+1)} \mathbf{C}^{(n+1)} \mathbf{A} \begin{bmatrix} 1 \\ \mathbf{b}^{(n+1)} \end{bmatrix} \right\} + \mathbf{n}_c^{(n)}$$

where, if we let $\mathbf{c}^{(n)} \equiv \left[c_{(0)}^{(n)} \cdots c_{(L-1)}^{(n)} \right]^T$ be the vector of the L complex channel amplitudes, $\mathbf{C}^{(n)} \equiv \mathbf{I}_{(K+1)} \otimes \mathbf{c}^{(n)}$ is the $(K + 1)L \times (K + 1)$ matrix of complex channel amplitudes ($\mathbf{X} \otimes \mathbf{Y}$ denotes the Kronecker tensor product of matrices $\mathbf{X}$ and $\mathbf{Y}$), $\mathbf{A}$ is the $(K + 1) \times (K + 1)$ diagonal matrix of real amplitudes whose k^{th} diagonal component is A_k ($k = 0 \ldots K$), and $\mathbf{b}^{(n)}$ is the K-vector of data channel bits for symbol n. The noise vector $\mathbf{n}_c^{(n)}$ is a

zero-mean complex Gaussian L-vector whose real and imaginary components have the distribution

$$\begin{bmatrix} \left\{\mathbf{n}_c^{(n)}\right\}^R \\ \left\{\mathbf{n}_c^{(n)}\right\}^I \end{bmatrix} \sim \eta\left(\begin{bmatrix} \mathbf{0}_L \\ \mathbf{0}_L \end{bmatrix}, \frac{\sigma^2}{A_0^2}\begin{bmatrix} \left\{\mathbf{R}_{[P,P]}^{(n)}\right\}^{(R)} & \left\{\mathbf{R}_{[P,P]}^{(n)}\right\}^{(I)} \\ -\left\{\mathbf{R}_{[P,P]}^{(n)}\right\}^{(I)} & \left\{\mathbf{R}_{[P,P]}^{(n)}\right\}^{(R)} \end{bmatrix}\right),$$

where $\mathbf{0}_L$ is an L-vector of zeros, $\{\mathbf{X}\}^{(R)} \equiv \frac{1}{2}(\mathbf{X} + \mathbf{X}^*)$ is the Hermitian part of $\mathbf{X}$ and $\{\mathbf{X}\}^{(I)} \equiv \frac{1}{2}(\mathbf{X} - \mathbf{X}^*)$ is the skew-Hermitian part of $\mathbf{X}$.

The rake matched filter output is the sum of the L demodulator finger outputs in (6) as given by

$$y_k^{(n)} \equiv \sum_{l=0}^{L-1} y_{k(l)}^{(n)} = \mathrm{Re}\left\{\hat{\mathbf{c}}^{(n)H}\mathbf{z}_k^{(n)}\right\} + n_{y_k}^{(n)}, \qquad (7)$$

where the noise vector has distribution

$$n_{y_k}^{(n)} \sim \eta\left(0, \sigma^2\left\{\hat{\mathbf{c}}^{(n)H}\mathbf{R}_{[k,k]}^{(n)}\hat{\mathbf{c}}^{(n)}\right\}^{(R)}\right) \qquad (8)$$

and where

$$\mathbf{z}_k^{(n)} \equiv \mathbf{R}_k^{(n)}\mathbf{C}^{(n)}\mathbf{A}\begin{bmatrix} 1 \\ \mathbf{b}^{(n)} \end{bmatrix} + \mathbf{R}_k^{(n-1)}\mathbf{C}^{(n-1)}\mathbf{A}\begin{bmatrix} 1 \\ \mathbf{b}^{(n-1)} \end{bmatrix} + \mathbf{R}_k^{(n+1)}\mathbf{C}^{(n+1)}\mathbf{A}\begin{bmatrix} 1 \\ \mathbf{b}^{(n+1)} \end{bmatrix} \qquad (9)$$

is the L vector signal component of the combiner input. The bit decision for data channel k is $\hat{b}_k^{(n)} = \mathrm{sgn}\left(y_k^{(n)}\right)$. Consequently, from (7) and (8) and setting $b_k^{(n)} = 1$, the bit error probability for the conventional receiver is

$$P_{conv,k}\left(\sigma, \hat{\mathbf{c}}^{(n)}, \mathbf{b}^{(n)}, \mathbf{b}^{(n-1)}, \mathbf{b}^{(n+1)}\right) = Q\left[\frac{\mathrm{Re}\left(\hat{\mathbf{c}}^{(n)H}\mathbf{z}_k^{(n)}\right)}{\sigma\sqrt{\left\{\hat{\mathbf{c}}^{(n)H}\mathbf{R}_{[k,k]}^{(n)}\hat{\mathbf{c}}^{(n)}\right\}^{(R)}}}\right]. \qquad (10)$$

Interference Subtraction Detector

Using the interference subtraction receiver, assuming perfect channel estimates, the input to the channel estimator and data demodulator contains no pilot signal contributions corresponding to the interfering multipath components. As Figure 7 shows, the pilot signals are reconstructed using the channel estimate $\hat{c}_{IS(l)}^{(n-1)}$ from the previous symbol interval. Ideally, the pilot signals should be reconstructed from the received signal using more recent channel estimates. The fading rate is typically slow enough, however, so that the channel does not change appreciably from symbol to symbol. The collection of L channel estimates is

$$\hat{\mathbf{c}}_{IS}^{(n)} \equiv \begin{bmatrix} \hat{c}_{IS(0)}^{(n)} \\ \vdots \\ \hat{c}_{IS(L-1)}^{(n)} \end{bmatrix} = \frac{1}{A_0}\begin{bmatrix} \left\langle \mathbf{p}_{(0)}^{(n)}, \mathbf{r}_{IS(0)}^{(n)} \right\rangle \\ \vdots \\ \left\langle \mathbf{p}_{(L-1)}^{(n)}, \mathbf{r}_{IS(L-1)}^{(n)} \right\rangle \end{bmatrix},$$

where $\mathbf{r}_{IS(l)}^{(n)}$ is the input to demodulator finger l, which is given by

$$\mathbf{r}_{IS(l)}^{(n)} = \mathbf{r}_{(l)}^{(n)} - A_0\sum_{j\neq l}\hat{c}_{IS(j)}^{(n-1)}\left[\mathbf{p}_{(j[l])}^{(n)} + \mathbf{p}_{(j[l])}^{(n-1)}[\mathrm{L}] + \mathbf{p}_{(j[l])}^{(n+1)}[\mathrm{R}]\right]. \qquad (11)$$

The demodulator finger output for path l weighted by the channel estimate for this path is

$$y_{IS,k(l)}^{(n)} = \mathrm{Re}\left\{\hat{c}_{IS(l)}^{(n)}\left\langle \mathbf{s}_{k(l)}^{(n)}, \mathbf{r}_{IS\ (l)}^{(n)} \right\rangle\right\}. \qquad (12)$$

Accordingly, the rake matched filter output for channel k is

$$y_{IS,k}^{(n)} \equiv \sum_{l=0}^{L-1} y_{IS,k(l)}^{(n)} = \sum_{l=0}^{L-1}\mathrm{Re}\left\{\hat{\mathbf{c}}_{IS}^{(n)H}\mathbf{z}_{\mathbf{IS,k}}^{(n)}\right\} + n_{y_{IS,k}}^{(n)}, \qquad (13)$$

where

$$\mathbf{z}_{IS,k}^{(n)} \equiv \mathbf{z}_k^{(n)} - A_0\left[\mathbf{R}_{[k,P]}^{(n)} + \mathbf{R}_{[k,P]}^{(n-1)} + \mathbf{R}_{[k,P]}^{(n+1)}\right]\hat{\mathbf{c}}_{IS}^{(n-1)},$$

$\mathbf{z}_k^{(n)}$ is defined in (9), and the complex noise vector has real and imaginary components with distribution

$$n_{y_{IS,k}}^{(n)} \sim \eta\left(0, \left\{\hat{\mathbf{c}}_{IS}^{(n)H}\mathbf{R}_{[k,k]}^{(n)}\hat{\mathbf{c}}_{IS}^{(n)}\right\}^{(R)}\right). \qquad (14)$$

The bit decision is $\hat{b}_{IS,k}^{(n)} = \mathrm{sgn}\left(y_{IS,k}^{(n)}\right)$, and it follows from (13) and (14) that the bit error rate is

$$P_{IS,k}\left(\sigma, \hat{\mathbf{c}}_{IS}^{(n)}, \mathbf{b}^{(n)}, \mathbf{b}^{(n-1)}, \mathbf{b}^{(n+1)}\right) = Q\left[\frac{\mathrm{Re}\left(\hat{\mathbf{c}}_{IS}^{(n)H} z_{IS,k}^{(n)}\right)}{\sigma\sqrt{\left\{\hat{\mathbf{c}}_{IS}^{(n)H}\mathbf{R}_{[k,k]}^{(n)}\hat{\mathbf{c}}_{IS}^{(n)}\right\}^{(R)}}}\right]. \quad (15)$$

Combined Interference Subtraction and Partial Decorrelating Detector

Lastly, for the combined interference subtraction and partial decorrelating detector shown in Figure 8, we assume that the desired user demodulates $N \le K$ multicode data channels. To provide motivation for the decorrelator, we assume that no background noise is present and that pilot cancellation is done using perfect channel estimates from the appropriate bit interval. Thus, (11) becomes

$$\begin{aligned}\mathbf{r}_{IS(l)}^{(n)} &= \mathbf{r}_{(l)}^{(n)} \\ &\quad - A_0 \sum_{j \neq l}\left[\hat{c}_{IS(j)}^{(n-1)}\mathbf{p}_{(j[l])}^{(n-1)}[\mathrm{L}] \right. \\ &\quad + \hat{c}_{IS(j)}^{(n)}\mathbf{p}_{(j[l])}^{(n)} \\ &\quad \left. + \hat{c}_{IS(j)}^{(n+1)}\mathbf{p}_{(j[l])}^{(n+1)}[\mathrm{R}]\right].\end{aligned}$$

We define the $NL \times NL$ matrix,

$$\mathbf{R}_N^{(n)} = \begin{bmatrix} \mathbf{R}_{[1,1]}^{(n)} & \mathrm{L} & \mathbf{R}_{[1,N]}^{(n)} \\ \mathrm{M} & & \mathrm{M} \\ \mathbf{R}_{[N,1]}^{(n)} & \mathrm{L} & \mathbf{R}_{[N,N]}^{(n)} \end{bmatrix},$$

for symbol n and the analogous matrices $\mathbf{R}_N^{(n\pm1)}$ for symbols $n \pm 1$. We can use (13) to write the collection of decision statistics for the N multicode channels as an N-vector given by

$$\begin{aligned}\bar{\mathbf{y}}_{IS}^{(n)} &\equiv \begin{bmatrix} \bar{y}_{IS,1}^{(n)} \\ \vdots \\ \bar{y}_{IS,N}^{(n)} \end{bmatrix} \\ &= \left\{\hat{\mathbf{C}}_{IS}^{(n)H}\left[\mathbf{R}_N^{(n)}\hat{\mathbf{C}}_{IS}^{(n)}\mathbf{A}_N\mathbf{b}_N^{(n)} \right.\right. \\ &\quad + \mathbf{R}_N^{(n-1)}\hat{\mathbf{C}}_{IS}^{(n-1)}\mathbf{A}_N\mathbf{b}_N^{(n-1)} \\ &\quad \left.\left. + \mathbf{R}_N^{(n+1)}\hat{\mathbf{C}}_{IS}^{(n+1)}\mathbf{A}_N\mathbf{b}_N^{(n+1)}\right]\right\}^{(R)},\end{aligned} \quad (16)$$

where $\hat{\mathbf{C}}_{IS}^{(n)} \equiv \mathbf{I}_N \otimes \hat{\mathbf{c}}_{IS}^{(n)}$ is the $NL \times N$ (perfectly estimated) complex channel amplitude matrix for symbol n and $\mathbf{A}_N$ is the diagonal $N \times N$ matrix of real amplitudes, where $\mathbf{b}_N^{(n)}$ is the N vector of data channel bits for symbol n. Because the channel estimates were assumed to be perfect, no pilot signal contributions exist in $\bar{\mathbf{y}}_{IS}^{(n)}$. Notice that because elements of the matrices $\mathbf{R}_N^{(n\pm1)}$ are predominately zeros, by taking a linear transformation of $\bar{\mathbf{y}}_{IS}^{(n)}$ with the matrix $\left[\mathbf{M}^{(n)}\right]^{-1}$ where $\mathbf{M}^{(n)} \equiv \left\{\hat{\mathbf{C}}_{IS}^{(n)H}\mathbf{R}_N^{(n)}\hat{\mathbf{C}}_{IS}^{(n)}\right\}^{(R)}$, the k^{th} element of the resulting N vector is simply $b_k^{(n)}$ plus some residual terms due to both the intersymbol interference and the other $K - N$ channels. As a result, the linear transformation decorrelates the MC channels from each other. For a large number of MC channels, this matrix inversion may be too computationally intensive for a mobile handset to calculate during each symbol. Because of the random spreading codes for the data channels, the correlation matrix $\mathbf{R}_N^{(n)}$ is strongly diagonal. Consequently, the correlation matrix of the combined multipath signals $\mathbf{M}^{(n)}$ is also strongly diagonal, and the decorrelator $\left[\mathbf{M}^{(n)}\right]^{-1}$ can be replaced by an approximation that is more easily computed. First, let $\mathbf{F}^{(n)}$ be the $N \times N$ diagonal matrix whose terms are the corresponding diagonal components of $\mathbf{M}^{(n)}$. Let $\mathbf{O}^{(n)} \equiv \mathbf{M}^{(n)} - \mathbf{F}^{(n)}$ be the off-diagonal terms of $\mathbf{M}^{(n)}$. Then a first-order approximation of $\left[\mathbf{M}^{(n)}\right]^{-1}$ is

$$\mathbf{U}_1^{(n)} \equiv \left[\mathbf{F}^{(n)}\right]^{-1} - \left[\mathbf{F}^{(n)}\right]^{-1}\mathbf{O}^{(n)}\left[\mathbf{F}^{(n)}\right]^{-1}.$$

The performance of this approximate decorrelator was analyzed for the case of $N = K$.[19]

Because the k^{th} diagonal term of $\mathbf{F}$ is $\hat{\mathbf{c}}_{IS}^{(n)H}\mathbf{R}_{[k,k]}^{(n)}\hat{\mathbf{c}}_{IS}^{(n)}$ and because $\mathbf{R}_{[k,k]}^{(n)}$ is strongly diagonal with ones on the diagonal, $\mathbf{F}^{(n)}$ is well-approximated by $\left\|\hat{\mathbf{c}}_{IS}^{(n)}\right\|^2\mathbf{I}_N$. Therefore, $\mathbf{U}_1^{(n)} \approx \left\|\hat{\mathbf{c}}_{PIC}^{(n)}\right\|^{-2}\mathbf{I}_N - \left\|\hat{\mathbf{c}}_{PIC}^{(n)}\right\|^{-4}\mathbf{O}^{(n)}$. Because the bit decision is independent of any scaling factors, we can disregard the common factor $\left\|\hat{\mathbf{c}}_{IS}^{(n)}\right\|^{-2}$, leaving us with a second approximation to the decorrelator

$$\mathbf{U}_2^{(n)} \equiv \mathbf{I}_N - \left\|\hat{\mathbf{c}}_{IS}^{(n)}\right\|^{-2}\mathbf{O}^{(n)}. \quad (17)$$

Returning to the practical case of imperfect pilot cancellation and background noise, the linear transformation will no longer decorrelate the MC channels perfectly. In addition to the residual terms mentioned above, contributions will be made in the decorrelator output due to the other MC channels, uncanceled pilot signals, and background noise. In general, however, the contributions due to the MC channels will be greatly reduced at the decorrelator output compared to the input. Rewriting (16) for this case, we have from (13)

$$\mathbf{y}_{IS}^{(n)} \equiv \begin{bmatrix} y_{IS,1}^{(n)} \\ \vdots \\ y_{IS,N}^{(n)} \end{bmatrix} = \left\{ \hat{\mathbf{C}}_{IS}^{(n)H} \mathbf{z}_{IS}^{(n)} \right\}^{(R)} + \mathbf{n}_{y_{IS}}^{(\mathbf{n})}, \quad (18)$$

where

$$\begin{aligned} \mathbf{z}_{IS}^{(n)} \equiv \Bigg(& \left[\mathbf{R}_{N;P}^{(n)} \mathbf{R}_{N}^{(n)} \right] \mathbf{C}_{N+1}^{(n)} \mathbf{A}_{N+1} \begin{bmatrix} 1 \\ \mathbf{b}_{N}^{(n)} \end{bmatrix} \\ & + \left[\mathbf{R}_{N;P}^{(n-1)} \mathbf{R}_{N}^{(n-1)} \right] \mathbf{C}_{N+1}^{(n-1)} \mathbf{A}_{N+1} \begin{bmatrix} 1 \\ \mathbf{b}_{N}^{(n-1)} \end{bmatrix} \\ & + \left[\mathbf{R}_{N;P}^{(n+1)} \mathbf{R}_{N}^{(n+1)} \right] \mathbf{C}_{N+1}^{(n+1)} \mathbf{A}_{N+1} \begin{bmatrix} 1 \\ \mathbf{b}_{N}^{(n+1)} \end{bmatrix} \\ & - A_0 \left[\mathbf{R}_{N;P}^{(n)} + \mathbf{R}_{N;P}^{(n-1)} + \mathbf{R}_{N;P}^{(n+1)} \right] \hat{\mathbf{c}}_{IS}^{(n-1)} \Bigg) \end{aligned}$$

is the NL-vector input to the N multipath combiners, $\hat{\mathbf{c}}_{IS}^{(n)}$ (and $\hat{\mathbf{C}}_{IS}^{(n)}$) are no longer noiseless, $\mathbf{C}_{N+1}^{(n)} \equiv \mathbf{I}_{N+1} \otimes \mathbf{c}^{(n)}$ is the $(N+1)\,L \times (N+1)$ complex channel amplitude matrix for symbol n (and similarly for symbols $n \pm 1$), the $NL \times L$ correlation matrices are defined as

$$\mathbf{R}_{N;P}^{(n)} \equiv \begin{bmatrix} \mathbf{R}_{[1,P]}^{(n)} \\ \mathbf{M} \\ \mathbf{R}_{[N,P]}^{(n)} \end{bmatrix}$$

$$\mathbf{R}_{N;P}^{(n-1)} \equiv \begin{bmatrix} \mathbf{R}_{[1,P]}^{(n-1)} \\ \mathbf{M} \\ \mathbf{R}_{[N,P]}^{(n-1)} \end{bmatrix}$$

$$\mathbf{R}_{N;P}^{(n+1)} \equiv \begin{bmatrix} \mathbf{R}_{[1,P]}^{(n+1)} \\ \mathbf{M} \\ \mathbf{R}_{[N,P]}^{(n+1)} \end{bmatrix},$$

and the noise vector has distribution

$$\mathbf{n}_{y_{IS}}^{(\mathbf{n})} \sim \eta\left(\mathbf{0}_N, \sigma^2 \mathbf{M}^{(n)} \right). \quad (19)$$

Using the decorrelator $\left[\mathbf{M}^{(n)} \right]^{-1}$, the output is

$$\mathbf{y}_{IS-DD}^{(n)} \equiv \left[\mathbf{M}^{(n)} \right]^{-1} \mathbf{y}_{IS}^{(n)} = \mathbf{z}_{IS-DD}^{(n)} + \mathbf{n}_{y_{IS-DD}}, \quad (20)$$

where

$$\mathbf{z}_{IS-DD}^{(n)} \equiv \left[\mathbf{M}^{(n)} \right]^{-1} \left\{ \hat{\mathbf{C}}_{IS}^{(n)H} \mathbf{z}_{IS}^{(n)} \right\}^{(R)} \quad (21)$$

and where the noise vector has distribution

$$\mathbf{n}_{y_{IS-DD}}^{(\mathbf{n})} \sim \eta\left(\mathbf{0}_N, \sigma^2 \left[\mathbf{M}^{(n)} \right]^{-1} \right). \quad (22)$$

The bit decision for channel k is

$$\hat{b}_{IS-DD,k}^{(n)} = \mathrm{sgn}\left(y_{IS-DD,k}^{(n)} \right).$$

Using (21) and (22), the bit error rate for the combined interference subtraction and decorrelating detector is

$$\begin{aligned} & P_{IS-DD,k}\left(\sigma, \hat{\mathbf{C}}_{IS}^{(n)}, \mathbf{b}^{(n)}, \mathbf{b}^{(n-1)}, \mathbf{b}^{(n+1)} \right) \\ & \quad = Q\left[\frac{\mathbf{z}_{IS-DD,k}^{(n)}}{\sigma \sqrt{\left\{ \left[\mathbf{M}^{(n)} \right]^{-1} \right\}_{(kk)}}} \right], \end{aligned} \quad (23)$$

where $\left[\mathbf{X} \right]_{(kk)}$ is the k^{th} diagonal element of $\mathbf{X}$.

Turning our attention to the approximation of the decorrelator $\mathbf{U}_2^{(n)}$ defined in (17), the output of the linear transformation is

$$\mathbf{y}_{IS-DD2}^{(n)} \equiv \mathbf{U}_2^{(n)} \mathbf{y}_{IS}^{(n)} = \mathbf{z}_{IS-DD2}^{(n)} + \mathbf{n}_{\mathbf{y_{IS-DD2}}}^{(n)}, \quad (24)$$

where

$$\mathbf{z}_{IS-DD2}^{(n)} \equiv \mathbf{U}_2^{(n)} \left\{ \hat{\mathbf{C}}_{IS}^{(n)H} \mathbf{z}_{IS}^{(n)} \right\}^{(R)} \quad (25)$$

and where the noise vector has distribution

$$\mathbf{n}_{y_{IS-DD2}} \sim \eta\left(\mathbf{0}_N, \sigma^2 \mathbf{U}_2^{(n)} \mathbf{M}^{(n)} \mathbf{U}_2^{(n)} \right). \quad (26)$$

The bit decision for channel k is $\hat{b}_{IS-DD2,k}^{(n)} = \mathrm{sgn}\left(y_{IS-DD2,k}^{(n)} \right)$. Using (24) and (26), the bit error rate for the combined interference subtraction and approximate decorrelating detector is

$$\begin{aligned} & P_{IS-DD,k}\left(\sigma, \hat{\mathbf{C}}_{IS}^{(n)}, \mathbf{b}^{(n)}, \mathbf{b}^{(n-1)}, \mathbf{b}^{(n+1)} \right) \\ & \quad = Q\left[\frac{\mathbf{z}_{IS-DD2,k}^{(n)}}{\sigma \sqrt{\left[\mathbf{U}_2^{(n)} \mathbf{M}^{(n)} \mathbf{U}_2^{(n)} \right]_{(kk)}}} \right]. \end{aligned} \quad (27)$$

Acknowledgments

The authors gratefully acknowledge the stimulating discussions with Dave Davis, Bharat Doshi, Richard Ejzak, John Kolchmeyer, Suhas Pai, Andrzej Partyka, Kirin Rege, Bob Resuta, Bob Servilio, Govind Shah, and Giovanni Vannucci. The continuous and active support from Ben Benjamin, Victor Lawrence, and George Zysman is deeply appreciated.

References

1. A. J. Viterbi, "Wireless Digital Communication: A View Based on Three Lessons Learned,'' *IEEE Communications Magazine*, IEEE Publishing Company, New York, Vol. 29, No. 9, September 1991, pp. 33-36.
2. K. S. Gilhousen, I. M. Jacobs, R. Padobani, A. J. Viterbi, L. A. Weaver, and C. E. Wheatley, "On the Capacity of a Cellular CDMA System,'' *IEEE Transactions on Vehicular Technology*, Vol. VT-40, No. 2, IEEE Publishing Company, New York, May 1991, pp. 303-312.
3. R. L. Pickholtz, D. L. Schilling, and L. B. Milstein, "Theory of Spread-Spectrum Communications – A Tutorial,'' *IEEE Transactions on Communications*, Vol. COM-30, No. 5, IEEE Publishing Company, New York, May 1982, pp. 855-884.
4. ITU-T Recommendation H.223/Annex A, "Multiplexing Protocol for Low-Bit-Rate Multimedia Communication in Error-Prone Environments," International Telecommunications Union, Geneva, Switzerland, 1996.
5. Chih-Lin I and R. D. Gitlin, "Multi-Code CDMA Wireless Personal Communications Networks,'' U. S. Patent No. 5442625; also in *Proceedings of ICC '95*, Seattle, Washington, pp. 1060-1064.
6. Chih-Lin I, G. P. Pollini, L. Ozarow, and R. D. Gitlin, "Performance of Multi-Code CDMA Wireless Personal Communications Networks,'' *Proceedings of VTC '95*, Chicago, Illinois, pp. 907-911.
7. Chih-Lin I and S. Nanda, "Fundamental Issues and Tradeoffs for Multimedia Services Over Wireless CDMA Networks,'' *Proceedings of IEEE MoMuCom-3*, Princeton, New Jersey, September 25-27, 1996.
8. Chih-Lin I and S. Nanda, "Load- and Interference-Based Demand Assignment (LIDA) for Integrated Services in CDMA Wireless Systems,'' *Proceedings of the IEEE GLOBECOM Conference*, London, England, 1996.
9. E. Tiedelman and E. Zehavi, "Multiple Code Structure For CDMA Forward Channel'' Proceedings of ICUPC, San Diego, California, 1994.
10. Chih-Lin I and K. K. Sabnani, "Variable Spreading Gain CDMA with Adaptive Control for True Packet Switching Wireless Network,'' *Proceedings of the IEEE International Conference on Communications*, Seattle, Washington, June 1995, pp. 725-730.
11. N. Amitay, "Resource Auction Multiple Access (RAMA): Efficient Method for Fast Resource Assignment in Decentralized Wireless PCS,'' *Electronic Letters*, Vol. 28, April 9, 1992, pp. 799-801.
12. M. Karol and Chih-Lin I, "A Protocol for Fast Resource Assignment in Wireless PCS,'' *Proceedings of the 4th PIMRC '93*, Yokohama, Japan, September 8-11, 1993, pp. 686-690.
13. N. D. Wilson, R. Ganesh, K. Joseph, and D. Raychaudhuri, "Packet CDMA Versus Dynamic TDMA for Multiple Access in an Integrated Voice/Data PCN,'' *IEEE Journal of Selected Areas in Communications*, Vol. JSAC-11, No. 6, IEEE Publishing Company, New York, August 1993, pp. 870-884.
14. H. Harmuth, *Transmission of Information by Orthogonal Functions*, Springer-Verlag, New York, 1969.
15. R. Lupas and S. Verdú, "Linear Multiuser Detectors for Synchronous CDMA Channels" *IEEE Transactions on Information Theory*, Vol. 35, No. 1, IEEE Publishing Company, New York, January 1989, pp. 123-136.
16. A. Duel-Hallen, "Decorrelating Decision Feedback Multiuser Detector for Synchronous Code-Division Multiple Access Channels," *IEEE Transactions on Communications*, Vol. 41, No. 2, February 1993, pp. 285-240.
17. P. Patel and J. Holtzman, "Analysis of a Simple Successive Interference Cancellation Scheme in a DC/CDMA System," *IEEE Journal on Selected Areas of Communications*, Vol. 12(5), IEEE Publishing Company, New York, June 1994, pp. 796-807.
18. S. Verdú and N. Mandayam, "Analysis of an Approximate Decorrelating Detector," *Wireless Personal Communications*, January 1997.
19. G. Fettweis and H. Meyr, "High Speed Parallel Viterbi Decoding: Algorithms and VLSI Architectures," *IEEE Communications Magazine*, May 1991, pp. 46-55.
20. Chih-Lin I, C. A. Webb, S. ten Brink, and H. C. Huang, "Rake Receiver Architectures for MC-CDMA," *Proceedings of the Sixth WINLAB Workshop*, New Brunswick, New Jersey, March 20-21, 1997.

(Manuscript approved December 1996)

CHIH-LIN I was formerly a member of technical staff in the Communications Science Research Lab at Bell Labs in Holmdel, New Jersey, where she conducted wireless and networking research. At her new company, she holds the position of director of wireless/access technology and infrastructure. She is responsible for defining new technologies' impact and implication on policy and strategic thrusts, as well as for coordinating the company's position on technologies and infrastructure. Ms. I has a B.S. in electronics engineering from Chiao-Tung University in Shin-Chu, Taiwan. In addition, she received an M.S. from Syracuse University in New York, and a Ph.D. from Stanford University in California, both in electrical engineering.

CHARLES A. WEBB III is a member of technical staff in the Advanced Video and Distributed Systems Technology Department at Bell Labs in Holmdel, New Jersey. His current responsibilities include CDMA mobile terminal design for high-speed data. Previously, he designed parts of a dual-mode CDMA ASIC. Mr. Webb received a B.S. degree in biomedical engineering from the Rensselaer Polytechnic Institute in Troy, New York, and he is now completing the curriculum for an M.S. in electrical engineering at Columbia University in New York City.

HOWARD C. HUANG is a member of technical staff in the Wireless Communications Systems Research Department at Bell Labs in Holmdel, New Jersey. His work includes research and development on CDMA systems and multiuser detection technology. Mr. Huang received a B.S.E.E. degree from Rice University in Houston, Texas, and a Ph.D. degree in electrical engineering from Princeton University in New Jersey.

STEPHAN TEN BRINK was a member of the Wireless Circuits and Systems Research Department at Bell Labs in Holmdel, New Jersey, as a visiting scientist. He was responsible for conducting research on enhanced CDMA communication systems. Currently, Mr. ten Brink is working on multiuser communication systems in the Institute of Telecommunications at the University of Stuttgart in Germany. He has a Vordiplom degree in electrical engineering from the university, and he is currently working toward his Diplom-Ingenieur and Ph.D.

SANJIV NANDA is acting technical manager in the Performance Analysis Department at Bell Labs in Holmdel, New Jersey. In this assignment, he is responsible for the design, modeling, and performance of Lucent Technologies' cellular systems. Mr. Nanda received a Ph.D. degree in electrical engineering from the Rensselaer Polytechnic Institute in Troy, New York.

RICHARD D. GITLIN is research vice president of the Communication Science Division of Bell Labs in Holmdel, New Jersey. His division conducts research in speech and image processing, wireless systems, access and photonic systems, and high-speed broadband networking with the goal of extending the limits of communications technologies to provide key innovations for Lucent Technologies. Additionally, he has conducted and led pioneering research and development in several areas of digital communications. Mr. Gitlin holds 39 patents and is the winner of several best paper awards. He received a doctorate in engineering science from Columbia University in New York and is both a Bell Labs and an IEEE Fellow. ◆